

1 **Estimates of micro-, nano-, and picoplankton contributions to**  
2 **particle export in the northeast Pacific**

3

4 **B. L. Mackinson<sup>1</sup>, S. B. Moran<sup>1</sup>, M. W. Lomas<sup>2</sup>, G. M. Stewart<sup>3</sup>, R. P. Kelly<sup>1</sup>**

5

6 [1] {Graduate School of Oceanography, University of Rhode Island, Narragansett, RI 02882,  
7 USA}

8

9 [2] {Bigelow Laboratory for Ocean Sciences, East Boothbay, ME 04544, USA}

10

11 [3] {Queens College and Graduate Center, City University of New York, Flushing, NY 11367,  
12 USA}

13

14 Correspondence to: B. L. Mackinson (bmackinson@my.uri.edu)

15

16 **Abstract**

17

18 The contributions of micro-, nano-, and picoplankton to particle export were estimated  
19 from measurements of size-fractionated particulate <sup>234</sup>Th, organic carbon, and phytoplankton  
20 indicator pigments obtained during five cruises between 2010 and 2012 along Line P in the  
21 subarctic northeast Pacific Ocean. Sinking fluxes of particulate organic carbon (POC) and  
22 indicator pigments were calculated from <sup>234</sup>Th-<sup>238</sup>U disequilibria and, during two cruises,  
23 measured by sediment trap at Ocean Station Papa. POC fluxes at 100 m ranged from 0.65 – 7.95  
24 mmol m<sup>-2</sup> d<sup>-1</sup>, similar in magnitude to previous results at Line P. Microplankton pigments  
25 dominate indicator pigment fluxes (averaging 69±19% of total pigment flux), while  
26 nanoplankton pigments comprised the majority of pigment standing stocks (averaging 64±23%  
27 of total pigment standing stock). Indicator pigment loss rates (the ratio of pigment export flux to  
28 pigment standing stock) point to preferential export of larger microplankton relative to smaller  
29 nano- and picoplankton. However, indicator pigments do not quantitatively trace particle export  
30 resulting from zooplankton grazing, which may be an important pathway for the export of small  
phytoplankton. These results have important implications for understanding the magnitude and

31 mechanisms controlling the biological pump at Line P in particular, and more generally in  
32 oligotrophic gyres and high-nutrient, low-chlorophyll regions where small phytoplankton  
33 represent a major component of the autotrophic community.

34

## 35 **1 Introduction**

36 Phytoplankton community structure exerts an important influence on the strength and  
37 efficiency of the biological pump (Michaels and Silver, 1988; Boyd and Newton, 1999; Thibault  
38 et al., 1999; Brew et al., 2009; Lomas and Moran, 2011). Small nano- and picoplankton  
39 dominate the phytoplankton community in the oligotrophic gyres and high-nutrient, low-  
40 chlorophyll (HNLC) oceanographic regions. It has traditionally been thought that small  
41 phytoplankton represent a relatively small fraction of the downward flux of particulate organic  
42 carbon (POC) relative to larger phytoplankton, such as diatoms, which are generally thought to  
43 contribute disproportionately to POC export (e.g., Michaels and Silver, 1988). Recent studies  
44 have challenged this idea, suggesting that small phytoplankton contribute **significantly** to POC  
45 export, possibly through aggregation and incorporation into fecal pellets (Richardson and  
46 Jackson, 2007; [Amacher et al., 2009](#); Stukel and Landry, 2010; [Lomas and Moran, 2011](#); [Stukel  
47 et al., 2013](#)). A better understanding of the controls on the relative importance of small  
48 phytoplankton in POC export is needed to refine our understanding of the magnitude and  
49 mechanisms controlling the biological pump, particularly as recent climate models predict an  
50 expansion of the oligotrophic gyres where small cells dominate (Irwin et al., 2006; Polovina et  
51 al., 2008; Morán et al., 2010).

52 Ocean Station Papa (OSP, 50°N, 145°W), the site of one of the longest-running ocean  
53 time-series, is located in the northeast Pacific Ocean in one of three major HNLC regions.  
54 Previous attempts to resolve the apparent paradox of low phytoplankton biomass and high nitrate  
55 concentrations at OSP concluded that a bottom-up control related to iron limitation is most  
56 important for large phytoplankton (Muggli et al., 1996; Harrison, 2006; Marchetti et al., 2006),  
57 while microzooplankton grazing exerts a strong top-down control on pico- and nanoplankton  
58 (Landry et al., 1993; Harrison et al., 1999; Rivkin et al., 1999). Primary production at the  
59 stations proximal to the coast on Line P (P4 & P12) is not iron-limited and diatom blooms are  
60 typically observed in spring and late summer (Boyd and Harrison, 1999; Thibault et al., 1999).  
61 At the offshore stations (including OSP) the phytoplankton community is dominated by cells <5-

Brendan Mackinson 1/17/2015 2:36 PM  
**Deleted:** in proportion to their contribution  
to biomass

64  $\mu\text{m}$  and the seasonal variability of primary production is relatively low ( $\sim 25 \text{ mmol C m}^{-2} \text{ d}^{-1}$  in  
65 winter and  $\sim 67 \text{ mmol C m}^{-2} \text{ d}^{-1}$  in summer) (Boyd and Harrison, 1999; Thibault et al., 1999;  
66 Choi et al., 2014). In contrast to the low variability in primary production, POC export recorded  
67 by moored sediment traps at OSP exhibits a stronger seasonal cycle with fluxes at 200 m depth  
68 ranging from  $\sim 0.4 \text{ mmol C m}^{-2} \text{ d}^{-1}$  in winter to  $\sim 2.4 \text{ mmol C m}^{-2} \text{ d}^{-1}$  in summer (Timothy et al.,  
69 2013). The average annual sediment trap POC flux at OSP ( $1.4 \pm 1.1 \text{ mmol C m}^{-2} \text{ d}^{-1}$ ) is nearly  
70 five times lower than the annual net community production (ANCP) at OSP ( $6.3 \pm 1.6 \text{ mmol C}$   
71  $\text{m}^{-2} \text{ d}^{-1}$ ), suggesting that the majority of organic carbon export is due to active transport by  
72 zooplankton and/or dissolved organic carbon (DOC) export (Timothy et al., 2013; Emerson,  
73 2014).

74 This study builds upon prior investigations of phytoplankton community composition and  
75 export production along Line P by examining the distributions of organic carbon, phytoplankton  
76 indicator pigments, and  $^{234}\text{Th}$  in three particle size-fractions. Sinking fluxes of POC and  
77 indicator pigments from the upper waters ( $\sim 100 \text{ m}$ ) were calculated from the  $^{234}\text{Th}$ – $^{238}\text{U}$   
78 disequilibrium and, during two cruises, measured at OSP using free-floating sediment traps. A  
79 comparison of indicator pigment fluxes with the respective standing stocks suggests that  
80 microplankton (20 – 200- $\mu\text{m}$ ) make up a higher percentage of particle export than biomass,  
81 whereas pico- and nano plankton (0.2 – 2- $\mu\text{m}$  and 2 – 20- $\mu\text{m}$ ) make up a lower percentage of  
82 particle export than biomass.

Brendan Mackinson 1/25/2015 3:27 PM  
Deleted: POC

Brendan Mackinson 1/25/2015 3:27 PM  
Deleted: POC

## 84 2 Methods

### 85 2.1 Study location

86 Sample collection was conducted at five stations along Line P (P4, P12, P16, P20, and  
87 P26 (OSP)) during cruises aboard the *CCGS John P. Tully* in August 2010, February 2011, June  
88 2011, February 2012, and June 2012 (Fig. 1, Table 1). Line P is located at the southern edge of  
89 the Alaskan Gyre, and the prevailing winds and surface currents are west-east (Bograd et al.,  
90 1999). Because precipitation and continental run-off exceed evaporation, a permanent halocline  
91 exists at  $\sim 100 \text{ m}$  impeding deep winter mixing. In addition, a seasonal thermocline forms at  $\sim 50$   
92  $\text{m}$  in spring and shoals to  $\sim 20 \text{ m}$  in summer (Freeland et al., 1997; Thibault et al., 1999;  
93 Freeland, 2013; Timothy et al., 2013).

94

97 **2.2 Net primary production by  $^{14}\text{C}$  incubation**

98 Rates of net primary production (NPP) were determined following the protocols outlined  
99 in Lomas et al. (2012). Samples were collected with Niskin bottles from seven depths in the  
100 euphotic zone corresponding to 1, 5, 9, 17, 33, 55, and 100% of surface irradiance. Three ‘light’  
101 bottles, a single ‘dark’ bottle, and a single initial ( $T_0$ ) bottle were each spiked with  $\sim 10 \mu\text{Ci}$   
102  $\text{NaH}^{14}\text{CO}_3$ . A sub-sample to confirm total added activity was removed from the  $T_0$  bottle at each  
103 light depth and immediately added to an equal volume of  $\beta$ -phenylethylamine. Bottles were  
104 incubated under simulated in situ conditions, using neutral density screening to mimic light  
105 levels at the depth of sample collection, in an on-deck incubator for  $\sim 24$  hours. After incubation,  
106 125 mL sub-samples from each light and dark bottle were filtered through an Ahlstrom 151 (0.7-  
107  $\mu\text{m}$  nominal pore size) and a Whatman Track Etch 5- $\mu\text{m}$  filter and rinsed with 10% HCl.  
108 Samples were counted on a Perkin Elmer TriCarb 2900LR  $\sim 48$  h after the addition of 5 mL of  
109 Ultima Gold (Perkin Elmer, USA) scintillation cocktail.  
110

111 **2.3 Water column  $^{234}\text{Th}$**

112 Total  $^{234}\text{Th}$  (dissolved + particulate) analysis followed the procedures outlined in Bauman  
113 et al. (2013). Briefly, samples (4 L) were collected by Niskin bottle at 12 depths (surface to  
114  $\sim 500$  m) and spiked with  $^{230}\text{Th}$  to monitor Th recovery. Samples were then treated with 7-8  
115 drops of concentrated  $\text{NH}_4\text{OH}$  solution, followed by 25  $\mu\text{L}$  of 0.2 M  $\text{KMnO}_4$ , and finally with  
116 11.5  $\mu\text{L}$  of 1.0 M  $\text{MnCl}_2$  to form a  $\text{MnO}_2$  precipitate that quantitatively scavenges Th (Benitez-  
117 Nelson et al., 2001; Buesseler et al., 2001; van der Loeff et al., 2006). After 1 hour, samples  
118 were vacuum filtered onto 25 mm glass microfiber filters (GM/F, 1- $\mu\text{m}$  nominal pore size) that  
119 were frozen for later analysis in the shore-based laboratory. To prepare samples for counting,  
120 filters were dried at  $50^\circ\text{C}$  for  $\sim 24$  hours, mounted on acrylic planchets, and covered with  
121 aluminum foil. To quantify  $^{234}\text{Th}$ , the beta emission of  $^{234\text{m}}\text{Pa}$  ( $E_{\text{max}} = 2.19 \text{ MeV}$ ;  $t_{1/2} = 1.2 \text{ min}$ )  
122 was counted using a RISØ National Laboratory low-background beta detector (Roskilde,  
123 Denmark). Each sample was counted four times over a period of approximately six half-lives,  
124 with the first count made at least 10 days after collection to allow for the decay of short-lived  
125 isotopes, and the final count used to quantify background levels. Data were fitted to the  $^{234}\text{Th}$   
126 decay curve to calculate the decay-corrected activity at the time of sample collection. Following  
127 the  $^{234}\text{Th}$  analysis, Th was radiochemically purified and  $^{230}\text{Th}$  was measured by alpha particle

128 [emission in order to determine scavenging efficiency. Small-volume scavenging efficiencies](#)  
129 [were found to be >90%. <sup>238</sup>U activities were calculated from salinity using the relationship <sup>238</sup>U](#)  
130 [= 0.07081 x S \(‰\) \(Chen et al., 1986\)](#)

131

#### 132 **2.4 Water column POC, Chl *a*, and indicator pigments**

133 Water samples for POC, Chl *a*, and phytoplankton indicator pigments were collected  
134 from the same depths in the photic zone as for NPP samples. Suspended POC was measured on  
135 1 L seawater samples filtered onto pre-combusted Ahlstrom 151 filters and frozen at -20°C until  
136 analysis. Samples were dried at 60°C in a drying oven, fumed in a desiccator containing  
137 concentrated hydrochloric acid for 24 h to remove inorganic carbonates, and dried again at 60°C.  
138 Samples were then analyzed on an EA-440 Analyzer (Exeter Analytical, Inc., Chelmsford, MA)  
139 (Pike and Moran, 1997). Chl *a* samples were analyzed using the methods outlined in Lomas et  
140 al. (2012). Separate samples (~0.2 L) were filtered onto Ahlstrom 151 and 5-µm Whatman  
141 Track Etch polycarbonate filters and frozen at -20°C until analysis. Samples were then extracted  
142 in 5 mL of 90% acetone for 24 h at -20°C and analyzed using a calibrated TD-700 fluorometer.

143 Indicator pigment samples were collected on separate Ahlstrom 151 filters and stored at -  
144 80°C until analysis by high-performance liquid chromatography (HPLC) at the Bermuda  
145 Institute of Ocean Sciences in the Bermuda Atlantic Time-series Study Laboratory (Knap et al.,  
146 1997). Fucoxanthin (FUCO), peridinin (PER), 19'-hexanoyloxyfucoxanthin (HEX), 19'-  
147 butanoyloxyfucoxanthin (BUT), alloxanthin (ALLO), total chlorophyll *b* (TChl *b*), and  
148 zeaxanthin (ZEA) were analyzed as indicator pigments based on their correspondence to  
149 particular phytoplankton taxonomic groups. Indicator proportion factors (PFs) were calculated  
150 to further analyze the size-distribution of the phytoplankton community (Hooker et al., 2005;  
151 Lomas and Moran, 2011). The sum of FUCO and PER concentrations was used to determine the  
152 microplankton proportion factor (mPF), while the sum of HEX, BUT, ALLO, and TChl *b* was  
153 used to determine the nanoplankton proportion factor (nPF), and ZEA was used to determine the  
154 picoplankton proportion factor (pPF) (Hooker et al., 2005; Lomas and Moran, 2011). Hooker et  
155 al. (2005) included TChl *b* in pPF, but because *Prochlorococcus* is not found in the study region,  
156 it was assumed in this study that any Chl *b* would be found in cells (e.g., chlorophytes and  
157 euglenophytes) in the nanoplankton size-class.

158

159 **2.5 In situ pump sampling**

160 Large-volume in situ pumps (Challenger Oceanic Systems and Services, UK and McLane  
161 Scientific, Falmouth, MA) were deployed for approximately four hours at depths of 30, 50, 100,  
162 150, and 200 m. Each pump sampled 100 – 1000 liters to collect size-fractionated particles, with  
163 seawater passing sequentially through 53- $\mu\text{m}$ , 10- $\mu\text{m}$ , and 1- $\mu\text{m}$  Nitex screens. Particles were  
164 resuspended by ultrasonication in 0.7- $\mu\text{m}$  prefiltered seawater and filtered onto separate pre-  
165 combusted GF/F filters for parallel analysis. Indicator pigment samples were stored at -80°C  
166 until analysis by high-performance liquid chromatography (HPLC) at the Bermuda Institute of  
167 Ocean Sciences in the Bermuda Atlantic Time-series Study Laboratory (Knap et al., 1997).  
168 Filters for analysis of POC and  $^{234}\text{Th}$  were frozen at -20°C until analysis. A sub-sample (~30%  
169 by weight) was cut with acetone-cleaned stainless steel scissors from each  $^{234}\text{Th}$  filter for POC  
170 analysis, and these sub-samples were dried and fumed with concentrated HCl as described  
171 above. POC was then measured using a CE 440 CHN Elemental Analyzer (Exeter Analytical,  
172 Inc., Chelmsford, MA). The  $^{234}\text{Th}$  filter subsample was dried at 60°C in a drying oven and  
173 counted on a RISØ beta detector as noted above.

174

175 **2.6 Sediment trap sampling**

176 Surface-tethered particle interceptor traps (PITS) with cylindrical tubes (KC-Denmark,  
177 Silkeborg, Denmark) were deployed for ~3 days at station P26 during the June 2011 and June  
178 2012 cruises to collect particles at the depths of 30, 50, 100, 150, and 200 m. Due to limited  
179 wire-time and other cruise constraints it was not possible to deploy sediment traps at any other  
180 stations sampled as part of this study. The trap design and sampling procedure is described in  
181 Baumann et al. (2012). Four tubes (72 mm diameter, 450 mm length) were used at each depth,  
182 and tubes were filled with non-poisoned, 0.4- $\mu\text{m}$  filtered brine ( $S = \sim 85 \text{ ‰}$ ) prior to deployment.  
183 Upon recovery trap brines were combined, particles were re-suspended and filtered onto pre-  
184 combusted GF/F filters, and swimmers were removed. Filters were stored frozen and later  
185 analyzed for POC,  $^{234}\text{Th}$ , and indicator pigments as described above.

186

187 **3 Results**

188 **3.1 Hydrography and NPP**

189 Depth sections of temperature and density anomaly ( $\sigma_t$ ) were generated using  
190 results from all CTD casts for a given cruise to improve horizontal data resolution (Fig. 2). The  
191 seasonal change in water temperature is largely confined to the upper ~100 m. Surface  
192 temperatures in August 2010 were ~14°C, while during the February cruises, surface  
193 temperatures were slightly cooler offshore (~6°C) than inshore (~8°C). During the June cruises,  
194 inshore temperatures were warmer (~10 – 12°C) while offshore temperatures remained relatively  
195 cool (~8°C). Density anomaly did not vary greatly between cruises below ~100 m. During the  
196 winter, a pool of less dense water (density of 1023 – 1025 kg m<sup>-3</sup>) was observed toward the coast  
197 (east of ~126°W). During the June cruises, this pool was observed extending west to ~130°W  
198 and during August 2010, it extended out to OSP (145°W). These data follow the expected  
199 seasonal pattern of a well-mixed water column in winter and increasing stratification moving  
200 from spring to summer.

201 Total NPP and >5- $\mu$ m size-fractionated NPP values were trapezoidally integrated over  
202 the euphotic zone (Table 2). A maximum total NPP of 91.9 mmol m<sup>-2</sup> d<sup>-1</sup> was measured at  
203 station P26 during June 2011, whereas the lowest value of 12.4 mmol m<sup>-2</sup> d<sup>-1</sup> was measured at  
204 station P26 during February 2012. These values agree to within a factor of two with the seasonal  
205 averages reported by Boyd and Harrison (1999). A maximum >5- $\mu$ m NPP of 39.6 mmol m<sup>-2</sup> d<sup>-1</sup>  
206 was at station P4 during June 2012 and a minimum of 2.2 mmol m<sup>-2</sup> d<sup>-1</sup> was measured at station  
207 P12 in February 2012.

208

### 209 **3.2 Small- and large-volume POC concentrations**

210 Suspended POC concentrations from Niskin bottle samples collected in the photic zone  
211 range from 1.1 – 7.1  $\mu$ mol L<sup>-1</sup>. POC concentrations were generally lowest at the base of the  
212 photic zone, though decreasing concentrations with depth were not observed at all stations (Table  
213 S1). The highest suspended POC concentrations were measured at station P4 during all cruises.  
214 POC concentrations were also measured in three size-fractions of particles collected with large-  
215 volume in situ pumps (Table S2). Concentrations of each size-fraction tended to decrease with  
216 depth and were typically less than 0.5  $\mu$ mol L<sup>-1</sup> at all depths. One exception was at station P26  
217 during February 2011 when POC concentrations at 30 m were between 1.8 and 2.9  $\mu$ mol L<sup>-1</sup> for  
218 all size-fractions.

219 The concentrations of POC collected using small-volume and large-volume methods  
220 often do not agree for samples collected at the same location and depth (Gardner, 1977; Moran et  
221 al., 1999; Liu et al., 2005; Liu et al., 2009). As reported in these previous studies, POC  
222 concentrations measured by large-volume in situ pumps (summed for all size-fractions) are  
223 significantly (ANOVA,  $p < 0.05$ ) less than small-volume POC measurements from the same  
224 station and similar depth (Fig. 3a). Explanations put forth to account for this discrepancy include  
225 DOC adsorption to filters, pressure effects on particle retention in pump samples, the collection  
226 of zooplankton by Niskin bottles but not pumps, and particle washout from pump filters (Moran  
227 et al., 1999; Liu et al., 2005; Liu et al., 2009). In this study, the smallest pump size-fraction  
228 was collected using a 1- $\mu\text{m}$  Nitex screen, not a GF/F, resulting in the pumps missing the portion  
229 of the POC on particles between 0.7- and 1- $\mu\text{m}$ , which may further contribute to the difference  
230 observed between the two methods. Lomas and Moran (2011) reported that sonication of in situ  
231 pump samples to resuspend particles from the Nitex screens had no significant effect on  
232 measured POC concentrations.

233

### 234 3.3 Particulate $^{234}\text{Th}$ and $\text{POC}/^{234}\text{Th}$ ratios

235 Size-fractionated particulate  $^{234}\text{Th}$  activities in samples collected by in situ pump  
236 generally decrease with depth, and are typically less than  $0.1 \text{ dpm L}^{-1}$  (Table S2). As with in situ  
237 pump POC concentrations, station P26 during February 2011 is an exception, with values  
238 exceeding  $0.1 \text{ dpm L}^{-1}$  for all size fractions at 30 m and throughout most of the water column for  
239 the 1 – 10- $\mu\text{m}$  fraction. Size-fractionated  $\text{POC}/^{234}\text{Th}$  ratios (Fig. 4, Table S2) are less than  $\sim 6$   
240  $\mu\text{mol dpm}^{-1}$  for all size-classes at most stations, with higher values measured at stations P4 and  
241 P12 in February 2012 and P4 in June 2012.  $\text{POC}/^{234}\text{Th}$  ratios tend to decrease or remain constant  
242 with depth, with one exception at station P12 during February 2012 where the maximum  
243  $\text{POC}/^{234}\text{Th}$  was at 100 m for all size fractions. Also, the  $\text{POC}/^{234}\text{Th}$  ratio does not vary greatly  
244 between size-fractions (Fig. 4) as was observed in Speicher et al. (2006) and Brew et al. (2009).

245 The accuracy of  $^{234}\text{Th}$  as a tracer of POC export depends on the assumption that  $^{234}\text{Th}$   
246 and POC are sinking on the same particles, and therefore sinking at the same rate (Moran et al.,  
247 2003; Smith et al., 2006; Speicher et al., 2006; Burd et al., 2007; Brew et al., 2009). A high  
248 degree of correlation between the size-fractionated distributions of  $^{234}\text{Th}$  and POC (Fig. 4) along  
249 Line P provides evidence in support of this assumption. All correlations were statistically

250 significant ( $p < 0.05$ ) and imply a strong coupling between particulate  $^{234}\text{Th}$  and POC for all  
251 cruises. In addition, the clustering of data for the different size-fractions of particles (Fig. 4)  
252 indicates that in February 2012 the 10 – 53- $\mu\text{m}$  size class contained the highest percentage of  
253 POC and particulate  $^{234}\text{Th}$ , while the  $>53\text{-}\mu\text{m}$  size class contained the lowest percentage. In June  
254 2012, the 1 – 10- $\mu\text{m}$  size class had the lowest percentage of POC and particulate  $^{234}\text{Th}$  while  
255 both the 10 – 53- $\mu\text{m}$  and the  $>53\text{-}\mu\text{m}$  fractions contained higher percentages (Fig. 4).

256

### 257 **3.4 Small-volume Chl *a* and indicator pigments**

258 Concentrations of total Chl *a* and  $>5\text{-}\mu\text{m}$  Chl *a* measured by fluorometer (Table S1) were  
259 trapezoidally integrated over the photic zone to determine respective standing stocks. During  
260 August 2010, the  $>5\text{-}\mu\text{m}$  fraction accounted for  $>30\%$  of the Chl *a* at all stations, with a  
261 maximum of 50% at station P26. During the other four cruises, the  $>5\text{-}\mu\text{m}$  size-fraction  
262 generally accounted for  $<30\%$  of the total Chl *a*, except at station P26 in February 2012 and  
263 station P4 in June 2012. Previous studies have reported that larger cells are more abundant at  
264 stations closer to the coast (Boyd and Harrison, 1999), though this was not always apparent. The  
265 highest  $>5\text{-}\mu\text{m}$  percentage of Chl *a* was measured at station P26 during August 2010, June 2011,  
266 and February 2012. Phytoplankton indicator pigments and Chl *a* concentrations in samples from  
267 the euphotic zone samples were also measured by HPLC (Table S1). HPLC and fluorescence  
268 Chl *a* concentrations generally agreed to within a factor of two, and the correlation between the  
269 two measurements was statistically significant ( $p < 0.05$ ) (Fig. S1). The correlation between the  
270 sum of the indicator pigment concentrations and the Chl *a* concentration was statistically  
271 significant ( $p < 0.05$ ) and roughly 1:1, suggesting that the indicator pigments examined in this  
272 analysis accounted for most of the phytoplankton biomass (Fig. S2). Furthermore, the  
273 correlation between the  $>5\text{-}\mu\text{m}$  fraction of Chl *a* and mPF is statistically significant ( $p < 0.05$ ),  
274 suggesting that this PF is a reasonable representation of that size-fraction of the phytoplankton  
275 community. Profiles of indicator pigment concentrations were trapezoidally integrated over the  
276 photic zone to quantify standing stocks (Table 3). FUCO was the most abundant microplankton  
277 pigment, and HEX was the most abundant nanoplankton pigment at most stations. Indicator  
278 pigment PFs (Fig. 5, Table S3) reveal that the phytoplankton community was typically  
279 dominated by nanoplankton, although at P4, and to a lesser extent at P20 in June 2012,  
280 microplankton pigments made up the bulk of the sample ( $\sim 86\%$  and  $\sim 52\%$  respectively).

281

### 282 3.5 Large-volume size-fractionated Chl *a* and indicator pigments

283 Size-fractionated Chl *a* and indicator pigment concentrations were also measured by in  
284 situ pump (Table S4). Chl *a* was once again strongly correlated in a roughly 1:1 ratio with the  
285 sum of the indicator pigments ( $p < 0.05$ ) (Fig. S3). The highest Chl *a* concentrations were  
286 measured in the 10 – 53- $\mu\text{m}$  fraction during all cruises. In February 2012, the >53- $\mu\text{m}$  fraction  
287 generally had the lowest concentrations, while in June 2012 and June 2011 the lowest  
288 concentrations were generally in the 1 – 10- $\mu\text{m}$  fraction.

289 Ideally, small-volume and large-volume concentrations of Chl *a* and indicator pigments  
290 should agree for samples collected at the same station and depth, but this was not observed in  
291 this study (Fig. 3). Although differences between small- and large-volume measurements of  
292 POC have been reported (Gardner, 1977; Moran et al., 1999; Liu et al., 2005; Liu et al., 2009),  
293 few studies have compared Niskin bottle and in situ pump measurements of indicator pigments  
294 (Lomas and Moran, 2011). Relative to bottle samples, the pump samples indicate higher  
295 concentrations of microplankton pigments FUCO and PER and lower concentrations of ZEA and  
296 TChl *b*, which are pigments associated with pico- and nanoplankton (Fig. 3b-d). Large-volume  
297 pump and small-volume bottle measurements of the nanoplankton indicator pigments HEX,  
298 BUT, and ALLO generally agree within a factor of two (Fig. 3b-d). Given the small size of  
299 ZEA-containing *Synechococcus* and TChl *b*-containing chlorophytes and prasinophytes, it is  
300 likely that many of these cells pass through the 1- $\mu\text{m}$  Nitex screen which would lead to under-  
301 sampling by the pumps (Liu et al., 2005). Bottles may undersample large, rare cells because the  
302 small volume might not be a statistically representative sample (Lomas and Moran, 2011).  
303 Furthermore, larger cells may settle below the spigot of the Niskin bottles, leading to a further  
304 bias against the collection of large cells (Gardner, 1977; Gundersen et al., 2001). Pumps sample  
305 higher concentrations of Chl *a* than bottles (Fig. 3a) at stations with high concentrations of Chl *a*,  
306 but when Chl *a* concentrations are low ( $<200 \text{ ng L}^{-1}$ ), the pumps tend to undersample relative to  
307 the bottles.

308 Given these sampling differences, it is important to note that although the total  
309 concentrations (summed for all size-fractions) measured by the in situ pumps may be inaccurate,  
310 it is still possible that the >53- $\mu\text{m}$  fraction accurately represents the composition of sinking  
311 particles. The disruption of loosely-bound aggregates during collection by the pumps could

312 cause an error in the >53- $\mu\text{m}$  fraction, but this is considered unlikely due to the presence of  
 313 nanoplankton (and in some cases picoplankton) pigments in this fraction. Furthermore, a recent  
 314 study in the Sargasso Sea employed a similar methodology and also found picoplankton  
 315 pigments in three particle size-classes, each >10- $\mu\text{m}$  (Lomas and Moran, 2011).

316 Indicator pigment PFs calculated for the size-fractionated particles (Table S3) and plotted  
 317 against depth (Figs. 6-8) reveal that while the overall indicator pigment concentrations vary with  
 318 depth and across size-fractions, the PFs do not exhibit a systematic pattern of variation across  
 319 size classes, depths, or seasons. The picoplankton pigment ZEA typically represents <10% of  
 320 the total indicator pigments for all size classes. Microplankton pigments dominated samples at  
 321 station P4 in February 2012 and June 2012, with mPFs typically exceeding 0.5 and 0.8,  
 322 respectively, for each cruise. In addition, mPFs were high at station P26 during these times, with  
 323 values generally exceeding 0.5 (Figs. 7-8). Nanoplankton pigments dominated at station P12 in  
 324 February 2012 cruise with nPFs exceeding 0.5 for most samples. As with the small volume  
 325 samples, FUCO was usually the most abundant microplankton pigment while HEX was usually  
 326 the most abundant nanoplankton pigment (Table S4).

327

### 328 **3.6 Total $^{234}\text{Th}$ , $^{234}\text{Th}/^{238}\text{U}$ activity ratios, and $^{234}\text{Th}$ fluxes**

329 Total (dissolved + particulate)  $^{234}\text{Th}$  activities,  $^{238}\text{U}$  activities, and  $^{234}\text{Th}/^{238}\text{U}$  activity  
 330 ratios are listed in Table S5. Depth sections of these  $^{234}\text{Th}/^{238}\text{U}$  activity ratios (Fig. 2d) indicate  
 331 that areas of low  $^{234}\text{Th}/^{238}\text{U}$  are prevalent in spring and summer and corresponding to periods  
 332 known to have high particle export in this region (Wong et al., 1999; Timothy et al., 2013).

333  $^{234}\text{Th}$  fluxes ( $P_{Th}$ ) were calculated using these  $^{234}\text{Th}/^{238}\text{U}$  results and a 2-D steady-state model of  
 334 the radiochemical balance for  $^{234}\text{Th}$  in the upper ocean,

335

$$336 \frac{\partial A_{Th}}{\partial t} = A_U \lambda_{Th} - A_{Th} \lambda_{Th} - P_{Th} + K_h \frac{\partial^2 A_{Th}}{\partial x^2} + U_h \frac{\partial A_{Th}}{\partial x} \quad (1)$$

337

338 where  $A_U$  is the activity of  $^{238}\text{U}$ ,  $\lambda_{Th}$  is the  $^{234}\text{Th}$  decay constant,  $A_{Th}$  is the activity of  $^{234}\text{Th}$ ,  $P_{Th}$  is  
 339 the vertical flux of  $^{234}\text{Th}$  on sinking particles,  $K_h$  is the eddy diffusion coefficient, and  $U_h$  is the  
 340 current velocity (Coale and Bruland, 1985; Charette et al., 1999). Assuming a steady-state

341  $(\partial A_{Th}/\partial t = 0)$  over several weeks to months, and that the diffusive flux of  $^{234}\text{Th}$  is small relative  
342 to advection and can therefore be ignored, the vertical flux of  $^{234}\text{Th}$  (in  $\text{dpm m}^{-2} \text{d}^{-1}$ ) is defined  
343 by,

$$344 \quad P_{Th} = \int_0^z \left[ \lambda_{Th}(A_U - A_{Th}) + U_h \frac{\partial A_{Th}}{\partial x} \right] dz \quad (2)$$

345  
346 where  $z$  is the depth of the water column over which the flux is measured. In this study, the  
347 gradient of thorium ( $\partial A_{Th}/\partial x$ ) was only measured in the east-west direction (along Line P).  
348 Therefore,  $x$  is the east-west distance across which the gradient will be measured and  $U_h$  is the  
349 east-west current velocity. Current velocities determined from 5-year seasonal averages of  
350 surface drifter data (available from Fisheries and Oceans Canada) were found to be  $6 \pm 4 \text{ cm s}^{-1}$   
351 for the February cruises,  $4 \pm 2 \text{ cm s}^{-1}$  for the June cruises, and  $5 \pm 3 \text{ cm s}^{-1}$  for the August cruise.  
352 These values agree well with the  $\sim 10 \text{ cm s}^{-1}$  value reported by McNally, (1981) and used by  
353 Charette et al., (1999). Given that the currents in the region generally flow west-east, and with  
354 no data at stations north and south of Line P, the north-south transport of  $^{234}\text{Th}$  by advection had  
355 to be assumed to be negligible. At stations P12, P16, and P20, the  $^{234}\text{Th}$  gradient was measured  
356 between the adjacent stations. For stations P4 and P26 (at either end of Line P), the gradient of  
357  $^{234}\text{Th}$  was determined from the adjacent station assuming a linear change extended beyond the  
358 measured transect.

359  
360  $^{234}\text{Th}$  fluxes ( $P_{Th}$ ) calculated using the 2-D model are within 5% of fluxes determined  
361 using a steady-state 1-D model that ignores advection (Fig. S4). This indicates that, under these  
362 assumptions, the vertical flux of  $^{234}\text{Th}$  on sinking particles is the dominant transport term.  
363 Consistent with previous studies,  $^{234}\text{Th}$  fluxes at all stations were higher during the August and  
364 June cruises than during the February cruises (Fig. 9a) (Charette et al., 1999). Also,  $^{234}\text{Th}$  fluxes  
365 did not exhibit a consistent trend along Line P.

### 366 3.7 $^{234}\text{Th}$ -derived POC fluxes

367 The POC/ $^{234}\text{Th}$  ratio in the  $>53\text{-}\mu\text{m}$  size-class and  $P_{Th}$  for a given depth horizon were  
368 used to calculate POC fluxes ( $P_{POC}$ ) (Fig. 9). In most cases,  $P_{POC}$  decreases with depth, although  
369 in some cases, the maximum  $P_{POC}$  in a given profile occurs at 50 or 100 m.  $P_{POC}$  fluxes at 100 m  
370 range from  $0.65 - 7.95 \text{ mmol m}^{-2} \text{d}^{-1}$ ; they are generally higher in summer than winter, and  
371

372 highest at station P4, consistent with previous studies at Line P (Charette et al., 1999; Wong et  
373 al., 1999; Timothy et al., 2013).

374 The ratio of  $P_{POC}$  flux to NPP, referred to as the  $ThE$ -ratio, is an estimate of efficiency of  
375 the biological pump (Buesseler, 1998).  $ThE$ -ratios determined using  $P_{POC}$  fluxes at the base of  
376 the photic zone (Table 2, Fig. 10) are similar to those reported by Charette et al. (1999), and are  
377 also in line with an annual average  $e$ -ratio determined using average sediment trap POC fluxes  
378 (Wong et al., 1999) and annual average NPP (Harrison, 2002) (Fig. 10).

379

### 380 3.8 Sediment trap $^{234}Th$ and POC fluxes

381 The particle fluxes of both  $^{234}Th$  and POC fluxes determined by the PITS traps ( $F_{Th}$  and  
382  $F_{POC}$  respectively) generally decrease with depth (Table 4).  $F_{Th}$  was higher in June 2012 than in  
383 June 2011, though there was no clear difference between the two cruises for  $F_{POC}$ . A comparison  
384 of the  $F_{Th}$  with the  $P_{Th}$  from corresponding stations and depths indicates that the  $F_{Th}$  is  
385 consistently higher than the  $P_{Th}$ , though usually not by more than a factor of two.  $F_{POC}$  is also  
386 consistently higher than  $P_{POC}$ , though again not by more than a factor of two (Fig. 11a). The  
387 POC/ $^{234}Th$  ratios of particles caught in sediment traps (Table 9) tend to be slightly higher  
388 (generally within a factor of 2) than the ratio of particles sampled by pumps at the corresponding  
389 station and depth.

390

### 391 3.9 $^{234}Th$ -derived and sediment trap pigment fluxes

392 Sinking fluxes of Chl  $a$  ( $P_{Chla}$ ) and indicator pigments ( $P_{Pigment}$ ) were calculated from  $P_{Th}$   
393 and the Pigment/ $^{234}Th$  ratio measured on  $>53\text{-}\mu\text{m}$  particles. Chl  $a$  and indicator pigment fluxes  
394 (Table 3, Fig. 12a-c) are generally highest at station P4 and decrease moving offshore. The  
395 highest indicator pigment fluxes were typically observed for microplankton pigments (FUCO  
396 and PER) whereas the lowest were observed for the picoplankton pigment ZEA (Table 3, Fig.  
397 12a-c). It is important to note that the differences between fluxes of different pigments at a given  
398 station are determined by the pigment ratio on the  $>53\text{-}\mu\text{m}$  particles and are independent of  $P_{Th}$ .

399 Sediment trap pigment fluxes ( $F_{Pigment}$ ) were typically lower than  $P_{Pigment}$  (Table 3, Fig.  
400 11b). The maximum sediment trap fluxes of Chl  $a$  and most indicator pigments were determined  
401 at 50 m in June 2011 and at 30 m in June 2012 (Table 3). For both deployments the deepest  
402 fluxes were generally the lowest, presumably due to the progressive degradation of sinking

Brendan Mackinson 1/15/2015 9:55 PM

Deleted: e

404 phytoplankton and resulting loss of pigments. Chl *a* and indicator pigment fluxes were generally  
405 higher in June 2011 than in June 2012, which is the opposite of the trend observed for  $F_{Th}$ .

406 Pigment PFs determined for material captured by the PITS traps do not vary greatly with  
407 depth, suggesting that the quality of material sinking to depth is similar to that in the surface  
408 water, despite the general decrease of material (Figs. 6 and 8). Microplankton PFs are higher for  
409 trap samples than for bottle samples but not as high as for pump samples, while nPFs and pPFs  
410 are higher for trap samples than for pump samples but lower than for bottle samples.

411

#### 412 **4 Discussion**

413 The results presented in this study build on previous investigations of export production  
414 in the northeast Pacific by providing estimates of the relative contributions of different  
415 phytoplankton size-classes to particle export. A comparison of indicator pigment standing stocks  
416 | **determined from small-volume samples** and  $P_{Pigment}$  fluxes suggests that while nanoplankton  
417 represented the bulk of phytoplankton biomass ( $68\pm 24\%$  of pigment standing stock, averaged for  
418 all stations and cruises), microplankton dominated the flux of pigmented material ( $69\pm 19\%$  on  
419 average) (Table 3, Fig. 12). Sediment trap pigment fluxes indicate a lower, but still substantial,  
420 relative contribution of microplankton to export, with microplankton pigments making up 47%  
421 and 33% of the total sediment trap indicator pigment flux in June 2011 and June 2012  
422 respectively, as compared to 81% and 85% of total  $P_{Pigment}$  fluxes. Though nano- and  
423 picoplankton did not form the majority of the algal aggregate flux, their  $29\pm 19\%$  contribution is  
424 significant and similar to contributions reported by Lomas and Moran (2011) for cyanobacteria  
425 and nano-eukaryotes in the Sargasso Sea.

426 Indicator pigment loss rates determined from both  $P_{Pigment}$  fluxes and sediment trap  
427 pigment fluxes imply that microplankton are exported more efficiently than nano- or  
428 picoplankton (Table 3, Fig. 12d-f). Loss rates of pigments, estimated as the ratio of  $P_{Pigment}$   
429 fluxes to pigment standing stock, averaged (for all cruises)  $8\pm 12\%$  for microplankton pigments,  
430  $1\pm 2\%$  for nanoplankton pigments and  $0.6\pm 1\%$  for picoplankton pigments. These results suggest  
431 that export of large cells by direct sinking of algal aggregates is more efficient than the export of  
432 small cells by the same pathway. Sediment trap loss rates for microplankton were also higher  
433 than those for nano- and picoplankton, further indicating preferential export of microplankton.  
434 Even though differences between bottle and pump samples may exaggerate the extent to which

435 large cells dominate export, sediment trap loss rates support and confirm the preferential export  
436 of large cells by algal aggregation.

437 In contrast to the trends observed for pigment fluxes and loss rates, the low variability of  
438 pump indicator pigment PFs with depth (Figs. 6-8) does not appear to indicate preferential export  
439 of microplankton. Furthermore, the presence of nano- and picoplankton pigments in the >53- $\mu\text{m}$   
440 size-fraction and in samples below the mixed layer suggests that nano- and picoplankton are  
441 incorporated into aggregates and that some of these aggregates are exported from the surface  
442 ocean. If large cells were being preferentially exported, microplankton pigments would be  
443 expected to make up a larger percentage of total pigments in samples below the mixed layer than  
444 in samples from the mixed layer, but this is not observed in the results of this study. It is  
445 possible that some of this discrepancy can be attributed to differences between bottle and pump  
446 samples. Because cells <1- $\mu\text{m}$  in size can pass through the 1- $\mu\text{m}$  Nitex screens used in the  
447 pumps, the sum of the pump size-fractions does not accurately reflect the community  
448 composition in the euphotic zone, and may miss a change in indicator pigment PFs with depth.  
449 In addition, the under-sampling of large cells by Niskin bottles may lead to an underestimate of  
450 microplankton standing stocks, and thus and overestimate of microplankton loss rates.

451 These pigment fluxes are likely lower estimates of the total contribution of each  
452 phytoplankton group to particle export. The use of indicator pigments as tracers of  
453 phytoplankton export only accounts for the direct sinking of healthy, ungrazed cells, because  
454 grazing degrades the indicator pigments to an analytically undetectable form (Head and Harris,  
455 1992; Strom et al., 1998; Thibault et al., 1999). Indirect export (via grazing) is thought to be an  
456 important pathway for picoplankton export in the HNLC Equatorial Pacific (Richardson et al.,  
457 2004; Stukel and Landry, 2010). Given that grazing has been shown to control the biomass of  
458 small phytoplankton in the northeast Pacific (Landry et al., 1993; Harrison et al., 1999; Rivkin et  
459 al., 1999), indirect export may also be a significant pathway for small cell export in this region.  
460 Because this pathway is not accounted for by the methodology employed in this study, the results  
461 presented here may underestimate the export of small phytoplankton, which may be less likely to  
462 sink directly.

463 Although grazing and fecal pellet export were not directly measured in this study, a  
464 comparison of sediment trap and pump measurements of Chl *a*, indicator pigments, and POC,  
465 suggests that zooplankton fecal pellets may be an important component of POC export at OSP, at

466 least in spring (Fig. 11). While  $F_{POC}$  fluxes are higher than the corresponding  $P_{POC}$  fluxes,  
467  $F_{Pigment}$  fluxes are lower than  $P_{Pigment}$  fluxes, indicating that the material captured by the sediment  
468 traps is enriched in carbon and depleted in Chl *a* and indicator pigments relative to that sampled  
469 by the pumps. Because the trap brine was not poisoned, zooplankton grazing and cell  
470 degradation in the trap tube may also have contributed to some loss of pigments over the ~3 day  
471 deployment of the PITS traps. However, the collection of carbon-rich and pigment-depleted  
472 fecal pellets by the traps but not by the pumps, which do not quantitatively sample fecal pellets  
473 (Lomas and Moran, 2011), could also explain these observations. This latter explanation is  
474 consistent with the results presented in Thibault et al. (1999), which indicate that fecal pellet  
475 export is 3 to 6 times greater than algal aggregate export at Line P.

476

## 477 **5 Conclusions**

478 New estimates of phytoplankton indicator pigment loss rates calculated from both  $^{234}\text{Th}$ -  
479 derived and sediment trap pigment fluxes suggest that large cells are preferentially exported at  
480 Line P. Specifically, microplankton pigments on average made up  $69\pm 19\%$  of the total pigment  
481 flux, but only  $32\pm 24\%$  of pigment standing stock ([determined from small-volume samples](#)),  
482 whereas nano- and picoplankton pigments on average formed  $31\pm 19\%$  of pigment flux in spite of  
483 representing  $68\pm 24\%$  of the standing stock. These results are consistent with traditional food  
484 web models (Michaels and Silver, 1988; Legendre and Le Fèvre, 1995) that suggest nano- and  
485 picoplankton are underrepresented in particle flux relative to their contribution to phytoplankton  
486 biomass; they also lend support to the conclusions of Choi et al. (2014). However, the methods  
487 employed in this study do not quantitatively account for export via zooplankton fecal pellets,  
488 which could be significant for small phytoplankton as they are controlled by grazing in this  
489 region (Landry et al., 1993; Harrison et al., 1999; Rivkin et al., 1999; Thibault et al., 1999).  
490 Furthermore, the determination of pigment loss rates also required a comparison between small-  
491 and large-volume samples, and the inherent differences of these sampling techniques likely led to  
492 an overestimation of the microplankton contribution to algal aggregate export. Therefore, it is  
493 possible that all sizes-classes of phytoplankton contribute to POC export in approximate  
494 proportion to their contribution to NPP as predicted by Richardson and Jackson (2007).

495 This study, conducted in a subarctic HNLC region, contributes to the ongoing discussion  
496 of small cell export that has largely focused on tropical and subtropical regions (Richardson et

497 al., 2004; Richardson et al., 2006; Richardson and Jackson, 2007; Stukel and Landry, 2010;  
498 Lomas and Moran, 2011). In particular, these results suggest that nano- and picoplankton may  
499 contribute significantly to POC export in this subarctic HNLC region, even if they are not as  
500 efficiently exported as larger microplankton. If large phytoplankton drive more efficient POC  
501 export in the northeast Pacific as suggested by this study, it could have important implications  
502 for understanding the biological pump. It has been proposed that decreasing winter mixed layer  
503 depths (Freeland et al., 1997; Freeland, 2013) and variations of macronutrient concentrations  
504 linked to shifts in climate regime (Pena and Varela, 2007) in the northeast Pacific could lead to  
505 shifts in the phytoplankton community composition. This study suggests that such changes in  
506 phytoplankton community composition could significantly affect the efficiency of the biological  
507 pump, and in turn, the cycling of carbon. While the results indicate that shifts in community  
508 composition favoring larger phytoplankton could lead to more efficient particle export, they do  
509 not indicate that shifts favoring smaller phytoplankton would lead to a shutdown of POC export  
510 as suggested by some previous studies (e.g., Michaels and Silver, 1988), but merely that the  
511 export of POC could be less efficient.

512

513 **Acknowledgements**

514 We thank the captain and crew of the CCGS *John P. Tully*, Marie Robert and the Line P Program  
515 collaborators, Doug Bell for at-sea sampling and laboratory assistance, and Matthew Baumann  
516 for his laboratory assistance. This research was supported by the National Science  
517 Foundation grants OCE 0926311 to SBM, OCE 0927559 to MWL, and OCE 0926348 to GMS.

518

519

520

521

522

523

524

525

526

527 |

528 **References**

- 529 [Amacher, J., Neuer, S., Anderson, I. and Massana, R.: Molecular approach to determine](#)  
530 [contributions of the protist community to particle flux, \*Deep-Sea Res. Part Oceanogr. Res. Pap.\*,](#)  
531 [56\(12\), 2206–2215, doi:10.1016/j.dsr.2009.08.007, 2009.](#)
- 532 [Baumann, M. S., Moran, S. B., Lomas, M. W., Kelly, R. P. and Bell, D. W.: Seasonal decoupling](#)  
533 [of particulate organic carbon export and net primary production in relation to sea-ice at the shelf](#)  
534 [break of the eastern Bering Sea: Implications for off-shelf carbon export, \*J. Geophys. Res.\*](#)  
535 [Oceans, 118\(10\), 5504–5522, doi:10.1002/jgrc.20366, 2013.](#)
- 536 [Benitez-Nelson, C. R., Buesseler, K. O., Van der Loeff, M. R., Andrews, J., Ball, L., Crossin, G.](#)  
537 [and Charette, M. A.: Testing a new small-volume technique for determining  \$^{234}\text{Th}\$  in seawater,](#)  
538 [J. Radioanal. Nucl. Chem., 248\(3\), 795–799, 2001.](#)
- 539 [Bograd, S. J., Thomson, R. E., Rabinovich, A. B. and LeBlond, P. H.: Near-surface circulation of](#)  
540 [the northeast Pacific Ocean derived from WOCE-SVP satellite-tracked drifters, \*Deep Sea Res.\*](#)  
541 [Part II Top. Stud. Oceanogr., 46\(11–12\), 2371 – 2403, doi:http://dx.doi.org/10.1016/S0967-](#)  
542 [0645\(99\)00068-5, 1999.](#)
- 543 [Boyd, P. and Harrison, P. J.: Phytoplankton dynamics in the {NE} subarctic Pacific, \*Deep Sea\*](#)  
544 [Res. Part II Top. Stud. Oceanogr., 46\(11–12\), 2405 – 2432, doi:http://dx.doi.org/10.1016/S0967-](#)  
545 [0645\(99\)00069-7, 1999.](#)
- 546 [Boyd, P. W. and Newton, P. P.: Does planktonic community structure determine downward](#)  
547 [particulate organic carbon flux in different oceanic provinces?, \*Deep Sea Res. Part Oceanogr.\*](#)  
548 [Res. Pap., 46\(1\), 63 – 91, doi:http://dx.doi.org/10.1016/S0967-0637\(98\)00066-1, 1999.](#)
- 549 [Brew, H. S., Moran, S. B., Lomas, M. W. and Burd, A. B.: Plankton community composition,](#)  
550 [organic carbon and thorium-234 particle size distributions, and particle export in the Sargasso](#)  
551 [Sea, \*J. Mar. Res.\*, 67\(6\), 845–868, doi:10.1357/002224009792006124, 2009.](#)
- 552 [Buesseler, K. O.: The decoupling of production and particulate export in the surface ocean, \*Glob.\*](#)  
553 [Biogeochem. Cycles, 12\(2\), 297–310, doi:10.1029/97GB03366, 1998.](#)
- 554 [Buesseler, K. O., Benitez-Nelson, C., Rutgers van der Loeff, M., Andrews, J., Ball, L., Crossin,](#)  
555 [G. and Charette, M. A.: An intercomparison of small-and large-volume techniques for thorium-](#)  
556 [234 in seawater, \*Mar. Chem.\*, 74\(1\), 15–28, 2001.](#)
- 557 [Burd, A. B., Jackson, G. A. and Moran, S. B.: The role of the particle size spectrum in estimating](#)  
558 [POC fluxes from disequilibrium, \*Deep Sea Res. Part Oceanogr. Res. Pap.\*, 54\(6\), 897–918, 2007.](#)
- 559 [Charette, M. A., Moran, S. B. and Bishop, J. K. B.:  \$^{234}\text{Th}\$  as a tracer of particulate organic carbon](#)  
560 [export in the subarctic northeast Pacific Ocean, \*Deep Sea Res. Part II Top. Stud. Oceanogr.\*,](#)  
561 [46\(11–12\), 2833 – 2861, doi:http://dx.doi.org/10.1016/S0967-0645\(99\)00085-5, 1999.](#)
- 562 [Chen, J. H., Lawrence Edwards, R. and Wasserburg, G. J.:  \$^{238}\text{U}\$ ,  \$^{234}\text{U}\$  and  \$^{232}\text{Th}\$  in seawater,](#)  
563 [Earth Planet. Sci. Lett., 80\(3\), 241–251, 1986.](#)

564 [Choi, H. Y., Stewart, G. M., Lomas, M. W., Kelly, R. P. and Moran, S. B.: Linking the](#)  
565 [distribution of <sup>210</sup>Po and <sup>210</sup>Pb with plankton community along Line P, Northeast Subarctic](#)  
566 [Pacific, J. Environ. Radioact., 2014.](#)

567 [Coale, K. H. and Bruland, K. W.: <sup>234</sup>Th: <sup>238</sup>U disequilibria within the California Current,](#)  
568 [Limnol Ocean., 30\(1\), 22–33, 1985.](#)

569 [Emerson, S.: Annual net community production and the biological carbon flux in the ocean,](#)  
570 [Glob. Biogeochem. Cycles, 2014.](#)

571 [Freeland, H., Denman, K., Wong, C. S., Whitney, F. and Jacques, R.: Evidence of change in the](#)  
572 [winter mixed layer in the Northeast Pacific Ocean, Deep Sea Res. Part Oceanogr. Res. Pap.,](#)  
573 [44\(12\), 2117 – 2129, doi:http://dx.doi.org/10.1016/S0967-0637\(97\)00083-6, 1997.](#)

574 [Freeland, H. J.: Evidence of Change in the Winter Mixed Layer in the Northeast Pacific Ocean:](#)  
575 [A Problem Revisited, Atmosphere-Ocean, 51\(1\), 126–133, 2013.](#)

576 [Gardner, W. D.: Incomplete extraction of rapidly settling particles from water samplers, Limnol](#)  
577 [Ocean., 22\(4\), 764–768, 1977.](#)

578 [Gundersen, K., Orcutt, K. M., Purdie, D. A., Michaels, A. F. and Knap, A. H.: Particulate](#)  
579 [organic carbon mass distribution at the Bermuda Atlantic Time-series Study \(BATS\) site, Deep](#)  
580 [Sea Res. Part II Top. Stud. Oceanogr., 48\(8\), 1697–1718, 2001.](#)

581 [Harrison, P. J.: SERIES \(subarctic ecosystem response to iron enrichment study\): A Canadian–](#)  
582 [Japanese contribution to our understanding of the iron–ocean–climate connection, Deep Sea Res.](#)  
583 [Part II Top. Stud. Oceanogr., 53\(20\), 2006.](#)

584 [Harrison, P. J., Boyda, P. W., Varela, D. E., Takeda, S., Shiomoto, A. and Odate, T.:](#)  
585 [Comparison of factors controlling phytoplankton productivity in the {NE} and {NW} subarctic](#)  
586 [Pacific gyres, Prog. Oceanogr., 43\(2–4\), 205 – 234, doi:http://dx.doi.org/10.1016/S0079-](#)  
587 [6611\(99\)00015-4, 1999.](#)

588 [Head, E. J. H. and Harris, L. R.: Chlorophyll and carotenoid transformation and destruction by](#)  
589 [Calanus spp. grazing on diatoms, Mar. Ecol.-Prog. Ser., 86, 229–229, 1992.](#)

590 [Hooker, S. B., Van Heukelem, L., Thomas, C. S., Claustre, H., Ras, J., Barlow, R., Sessions, H.,](#)  
591 [Schlüter, L., Perl, J. and Trees, C.: Second SeaWiFS HPLC Analysis Round-robin Experiment](#)  
592 [\(SeaHARRE-2\), National Aeronautics and Space Administration, Goddard Space Flight Center.,](#)  
593 [2005.](#)

594 [Irwin, A. J., Finkel, Z. V., Schofield, O. M. E. and Falkowski, P. G.: Scaling-up from nutrient](#)  
595 [physiology to the size-structure of phytoplankton communities, J. Plankton Res., 28\(5\), 459–471,](#)  
596 [doi:10.1093/plankt/fbi148, 2006.](#)

597 [Knap, A. H., Michaels, A. F., Steinberg, D. K., Bahr, F., Bates, N. R., Bell, S., Countway, P.,](#)  
598 [Close, A. R., Doyle, A. P. and Dow, R. L.: BATS Methods manual, version 4., 1997.](#)

599 [Landry, M. R., Monger, B. C. and Selph, K. E.: Time-dependency of microzooplankton grazing](#)  
600 [and phytoplankton growth in the subarctic Pacific, \*Prog. Oceanogr.\*, 32\(1–4\), 205 – 222,](#)  
601 [doi:http://dx.doi.org/10.1016/0079-6611\(93\)90014-5, 1993.](#)

602 [Legendre, L. and Le Fèvre, J.: Microbial food webs and the export of biogenic carbon in oceans,](#)  
603 [Aquat. Microb. Ecol., 9\(1\), 69–77, 1995.](#)

604 [Liu, Z., Cochran, J. K., Lee, C., Gasser, B., Miquel, J. C. and Wakeham, S. G.: Further](#)  
605 [investigations on why {POC} concentrations differ in samples collected by Niskin bottle and in](#)  
606 [situ pump, \*Deep Sea Res. Part II Top. Stud. Oceanogr.\*, 56\(18\), 1558 – 1567,](#)  
607 [doi:http://dx.doi.org/10.1016/j.dsr2.2008.12.019, 2009.](#)

608 [Liu, Z., Stewart, G., Kirk Cochran, J., Lee, C., Armstrong, R. A., Hirschberg, D. J., Gasser, B.](#)  
609 [and Miquel, J.-C.: Why do POC concentrations measured using Niskin bottle collections](#)  
610 [sometimes differ from those using in-situ pumps?, \*Deep Sea Res. Part Oceanogr. Res. Pap.\*,](#)  
611 [52\(7\), 1324–1344, doi:10.1016/j.dsr.2005.02.005, 2005.](#)

612 [Van der Loeff, M. R., Sarin, M. M., Baskaran, M., Benitez-Nelson, C., Buesseler, K. O.,](#)  
613 [Charette, M., Dai, M., Gustafsson, Ö., Masque, P. and Morris, P. J.: A review of present](#)  
614 [techniques and methodological advances in analyzing <sup>234</sup>Th in aquatic systems, \*Mar. Chem.\*,](#)  
615 [100\(3\), 190–212, 2006.](#)

616 [Lomas, M. W. and Moran, S. B.: Evidence for aggregation and export of cyanobacteria and](#)  
617 [nano-eukaryotes from the Sargasso Sea euphotic zone, \*Biogeosciences\*, 8\(1\), 203–216,](#)  
618 [doi:10.5194/bg-8-203-2011, 2011.](#)

619 [Lomas, M. W., Moran, S. B., Casey, J. R., Bell, D. W., Tiahlo, M., Whitefield, J., Kelly, R. P.,](#)  
620 [Mathis, J. T. and Coklet, E. D.: Spatial and seasonal variability of primary production on the](#)  
621 [Eastern Bering Sea shelf, \*Deep Sea Res. Part II Top. Stud. Oceanogr.\*, 65–70\(0\), 126 – 140,](#)  
622 [doi:http://dx.doi.org/10.1016/j.dsr2.2012.02.010, 2012.](#)

623 [Marchetti, A., Sherry, N. D., Kiyosawa, H., Tsuda, A. and Harrison, P. J.: Phytoplankton](#)  
624 [processes during a mesoscale iron enrichment in the NE subarctic Pacific: Part I—biomass and](#)  
625 [assemblage, \*Deep Sea Res. Part II Top. Stud. Oceanogr.\*, 53\(20\), 2095–2113, 2006.](#)

626 [McNally, G. J.: Satellite - tracked drift buoy observations of the near - surface flow in the](#)  
627 [eastern mid - latitude North Pacific, \*J. Geophys. Res. Oceans\* 1978–2012, 86\(C9\), 8022–8030,](#)  
628 [1981.](#)

629 [Michaels, A. F. and Silver, M. W.: Primary production, sinking fluxes and the microbial food](#)  
630 [web, \*Deep Sea Res. Part Oceanogr. Res. Pap.\*, 35\(4\), 473 – 490,](#)  
631 [doi:http://dx.doi.org/10.1016/0198-0149\(88\)90126-4, 1988.](#)

632 [Moran, S. B., Charette, M. A., Pike, S. M. and Wicklund, C. A.: Differences in seawater](#)  
633 [particulate organic carbon concentration in samples collected using small-and large-volume](#)  
634 [methods: the importance of DOC adsorption to the filter blank, \*Mar. Chem.\*, 67\(1\), 33–42, 1999.](#)

635 [Moran, S. B., Weinstein, S. E., Edmonds, H. N., Smith, J. N., Kelly, R. P., Pilson, M. E. Q. and](#)  
636 [Harrison, W. G.: Does  \$^{234}\text{Th}/^{238}\text{U}\$  disequilibrium provide an accurate record of the export flux](#)  
637 [of particulate organic carbon from the upper ocean?, \*Limnol. Oceanogr.\*, 48\(3\), 1018–1029,](#)  
638 [2003.](#)

639 [Morán, X. A. G., López-Urrutia, Á., Calvo - Díaz, A. and Li, W. K.: Increasing importance of](#)  
640 [small phytoplankton in a warmer ocean, \*Glob. Change Biol.\*, 16\(3\), 1137–1144, 2010.](#)

641 [Muggli, D. L., Lecourt, M. and Harrison, P. J.: Effects of iron and nitrogen source on the sinking](#)  
642 [rate, physiology and metal composition of an oceanic diatom from the subarctic Pacific,](#)  
643 [Oceanogr. Lit. Rev., 43\(11\), 1996.](#)

644 [Pena, M. A. and Varela, D. E.: Seasonal and interannual variability in phytoplankton and nutrient](#)  
645 [dynamics along Line P in the NE subarctic Pacific, \*Prog. Oceanogr.\*, 75\(2\), 200–222, 2007.](#)

646 [Polovina, J. J., Howell, E. A. and Abecassis, M.: Ocean's least productive waters are expanding,](#)  
647 [Geophys. Res. Lett., 35\(3\), 2008.](#)

648 [Richardson, T. L. and Jackson, G. A.: Small phytoplankton and carbon export from the surface](#)  
649 [ocean, \*Science\*, 315\(5813\), 838–840, 2007.](#)

650 [Richardson, T. L., Jackson, G. A., Ducklow, H. W. and Roman, M. R.: Carbon fluxes through](#)  
651 [food webs of the eastern equatorial Pacific: an inverse approach, \*Deep Sea Res. Part Oceanogr.\*](#)  
652 [Res. Pap., 51\(9\), 1245–1274, doi:10.1016/j.dsr.2004.05.005, 2004.](#)

653 [Richardson, T. L., Jackson, G. A., Ducklow, H. W. and Roman, M. R.: Spatial and seasonal](#)  
654 [patterns of carbon cycling through planktonic food webs of the Arabian Sea determined by](#)  
655 [inverse analysis, US JGOFS Synth. Model. Proj. Phase III US JGOFS Synth. Model. Proj. Phase](#)  
656 [III, 53\(5–7\), 555–575, doi:10.1016/j.dsr2.2006.01.015, 2006.](#)

657 [Rivkin, R. B., Putland, J. N., Robin Anderson, M. and Deibel, D.: Microzooplankton bacterivory](#)  
658 [and herbivory in the NE subarctic Pacific, \*Deep Sea Res. Part II Top. Stud. Oceanogr.\*, 46\(11\),](#)  
659 [2579–2618, 1999.](#)

660 [Speicher, E. A., Moran, S. B., Burd, A. B., Delfanti, R., Kaberi, H., Kelly, R. P., Papucci, C.,](#)  
661 [Smith, J. N., Stavrakakis, S. and Torricelli, L.: Particulate organic carbon export fluxes and size-](#)  
662 [fractionated POC/ \$^{234}\text{Th}\$  ratios in the Ligurian, Tyrrhenian and Aegean Seas, \*Deep Sea Res. Part\*](#)  
663 [Oceanogr. Res. Pap., 53\(11\), 1810–1830, 2006.](#)

664 [Strom, S., Morello, T. and Bright, K.: Protozoan size influences algal pigment degradation](#)  
665 [during grazing, \*Mar. Ecol. Prog. Ser. Halstenbek\*, 164, 189–197, doi:10.3354/meps164189,](#)  
666 [1998.](#)

667 [Stukel, M. R., Décima, M., Selph, K. E., Taniguchi, D. A. and Landry, M. R.: The role of](#)  
668 [Synechococcus in vertical flux in the Costa Rica upwelling dome, \*Prog. Oceanogr.\*, 112, 49–59,](#)  
669 [2013.](#)

670 [Stukel, M. R. and Landry, M. R.: Contribution of picophytoplankton to carbon export in the](#)  
671 [equatorial Pacific: A reassessment of food web flux inferences from inverse models, \*Limnol.\*](#)  
672 [Oceanogr., 55\(6\), 2669–2685, 2010.](#)

673 [Thibault, D., Roy, S., Wong, C. S. and Bishop, J. K.: The downward flux of biogenic material in](#)  
674 [the NE subarctic Pacific: importance of algal sinking and mesozooplankton herbivory, \*Deep Sea\*](#)  
675 [Res. Part II Top. Stud. Oceanogr., 46\(11\), 2669–2697, 1999.](#)

676 [Timothy, D. A., Wong, C. S., Barwell-Clarke, J. E., Page, J. S., White, L. A. and Macdonald, R.](#)  
677 [W.: Climatology of sediment flux and composition in the subarctic Northeast Pacific Ocean with](#)  
678 [biogeochemical implications, \*Prog. Oceanogr.\*, 116, 95–129, 2013.](#)

679 [Wong, C. S., Whitney, F. A., Crawford, D. W., Iseki, K., Matear, R. J., Johnson, W. K., Page, J.](#)  
680 [S. and Timothy, D.: Seasonal and interannual variability in particle fluxes of carbon, nitrogen](#)  
681 [and silicon from time series of sediment traps at Ocean Station P, 1982–1993: Relationship to](#)  
682 [changes in subarctic primary productivity, \*Deep Sea Res. Part II Top. Stud. Oceanogr.\*, 46\(11\),](#)  
683 [2735–2760, 1999.](#)

684  
685  
686  
687  
688  
689  
690  
691  
692  
693  
694  
695  
696  
697  
698  
699  
700

Table 1: Cruise dates and sample collection along Line P

<a href="#">Cruise Dates</a>	<a href="#">P4</a>	<a href="#">P12</a>	<a href="#">P16</a>	<a href="#">P20</a>	<a href="#">P26</a>
<a href="#">2010-14</a>	<a href="#">Total Th</a>				

<u>Aug. 2010</u>	-	-	-	-	-
<u>(8/19/10 - 8/31/10)</u>	-	<u>WC Pig</u>	<u>WC Pig</u>	<u>WC Pig</u>	-
<u>2011-01</u>	-	<u>Total Th</u>	<u>Total Th</u>	<u>Total Th</u>	<u>Total Th</u>
<u>Feb. 2011</u>	-	<u>WC Pig</u>	<u>WC Pig</u>	<u>WC Pig</u>	-
<u>(2/9/11 - 2/15/11)</u>	-	<u>WC Pig</u>	<u>WC Pig</u>	<u>WC Pig</u>	-
<u>2011-26</u>	<u>Total Th</u>				
<u>June 2011</u>	-	-	-	-	<u>Part. Th</u>
<u>(6/4/11 - 6/16/11)</u>	<u>WC Pig</u>				
-	-	-	-	-	<u>Part. Pig</u>
-	-	-	-	-	<u>Traps</u>
<u>2012-01</u>	<u>Total Th</u>				
<u>Feb. 2012</u>	<u>Part. Th</u>	<u>Part. Th</u>	-	-	<u>Part. Th</u>
<u>(2/7/12 - 2/19/12)</u>	<u>WC Pig</u>	<u>WC Pig</u>	-	-	<u>WC Pig</u>
-	<u>Part. Pig</u>	<u>Part. Pig</u>	-	-	<u>Part. Pig</u>
<u>2012-12</u>	<u>Total Th</u>				
<u>June 2012</u>	<u>Part. Th</u>				
<u>(5/23/12 - 6/7/12)</u>	<u>WC Pig</u>	<u>WC Pig</u>	<u>WC Pig</u>	-	-
-	<u>Part. Pig</u>				
-	-	-	-	-	<u>Traps</u>

701  
702  
703  
704  
705  
706  
707  
708  
709  
710  
711

Table 2: Total net primary production (NPP) and >5  $\mu\text{m}$  size-fractionated NPP determined from simulated in situ incubations.  
<sup>234</sup>Th-derived POC flux ( $P_{\text{POC}}$ ) and sediment trap POC flux ( $\text{Trap}_{\text{POC}}$ ) determined at the base of the photic zone and the corresponding  $\text{ThE}$ -ratios ( $P_{\text{POC}}/\text{NPP}$ ) and trap  $e$ -ratios ( $\text{Trap}_{\text{POC}}/\text{NPP}$ ).

<u>Cruise</u>	<u>Station</u>	<u>Integration Depth (m)</u>	<u>Total NPP (mmol m<sup>-2</sup> d<sup>-1</sup>)</u>	<u>&gt;5 μm NPP (mmol m<sup>-2</sup> d<sup>-1</sup>)</u>	<u>P<sub>POC</sub> (mmol m<sup>-2</sup> d<sup>-1</sup>)</u>	<u>Trapp<sub>POC</sub> (mmol m<sup>-2</sup> d<sup>-1</sup>)</u>	<u>ThE-ratio</u>	<u>Trap e-ratio</u>
<u>Feb. 2011</u>	<u>P20</u>	<u>77</u>	<u>36.64</u>	<u>3.26</u>				
<u>June 2011</u>	<u>P26-D</u>	<u>83</u>	<u>105.14</u>	<u>13.67</u>	<u>2.94</u>	<u>5.91</u>	<u>0.03</u>	<u>0.06</u>
	<u>P26-R</u>	<u>85</u>	<u>78.75</u>	<u>12.98</u>	<u>2.75</u>	<u>5.91</u>	<u>0.03</u>	<u>0.08</u>
<u>Feb. 2012</u>	<u>P4</u>	<u>50</u>	<u>27.91</u>	<u>3.58</u>	<u>7.29</u>		<u>0.26</u>	
	<u>P12</u>	<u>95</u>	<u>34.56</u>	<u>4.58</u>	<u>4.65</u>		<u>0.13</u>	
	<u>P26</u>	<u>75</u>	<u>23.41</u>	<u>5.22</u>	<u>0.31</u>		<u>0.01</u>	
<u>June 2012</u>	<u>P4</u>	<u>103</u>	<u>82.36</u>	<u>39.55</u>	<u>7.95</u>		<u>0.10</u>	
	<u>P12</u>	<u>164</u>	<u>40.24</u>	<u>4.16</u>	<u>2.12</u>		<u>0.05</u>	
	<u>P20</u>	<u>115</u>	<u>57.84</u>	<u>4.10</u>	<u>0.54</u>		<u>0.01</u>	
-	<u>P26</u>	<u>60</u>	<u>49.45</u>	<u>9.28</u>	<u>2.96</u>	<u>6.55</u>	<u>0.06</u>	<u>0.13</u>

712  
713  
714  
715  
716  
717  
718  
719  
720  
721  
722  
723  
724

Table 3: Chl *a* and indicator pigment standing stocks determined by integrating small volume pigment concentrations (determined by HPLC) across the photic zone, pigment fluxes (<sup>234</sup>Th and PITS-derived) measured at the base of the photic zone, and pigment loss rates, or the percent of the surface concentration represented by those fluxes. Pigment standing stocks are in mg m<sup>-2</sup> and pigment fluxes are in mg m<sup>-2</sup> d<sup>-1</sup>.

Cruise	Station	Depth	Chl <i>a</i>	FUCO	PER	HEX	BUT	ALLO	Chl <i>b</i>	ZEA
Aug. 2010 (2010-14)	P12	Surface (1-75 m)	23.918	3.498	0.375	7.705	1.165	0.220	4.038	1.435
	P16	Surface (1-75 m)	14.165	1.288	0.340	6.010	1.018	0.065	2.588	0.165
	P20	Surface (1-75 m)	19.040	3.138	0.398	6.298	1.453	0.065	2.620	0.188
Feb. 2011 (2011-01)	P12	Surface (1-65 m)	30.122	2.848	0.379	5.630	2.431	0.838	7.133	0.922
	P16	Surface (1-95 m)	16.230	1.286	0.202	5.728	1.726	0.161	4.439	1.643
	P20	Surface (1-77 m)	55.053	5.207	0.689	18.064	6.697	1.116	11.435	4.516
June 2011 (2011-26)	P4	Surface (1-72 m)	29.791	2.635	0.127	10.619	2.663	0.720	5.836	5.234
	P12	Surface (1-90 m)	26.115	5.060	0.085	11.988	3.263	0.498	2.665	3.063
	P16	Surface (1-105 m)	22.088	4.044	0.104	11.390	2.195	0.181	2.612	1.569
	P20	Surface (1-70 m)	19.421	4.423	0.197	8.132	1.913	0.166	2.090	1.129
	P26	Surface (1-84 m)	29.376	7.239	0.184	10.532	4.406	0.232	3.723	2.663
		Flux at 100 m	0.765	0.474	0.036	0.059	0.0002	0.016	0.028	0.018
	% Flux	2.605	6.548	$\frac{19.76}{2}$	0.564	0.004	6.686	0.753	0.658	
P26	Trap (150 m)	0.125	0.056	0.027	0.049	0.014	-	0.017	0.015	
	% Flux	0.424	0.767	$\frac{14.87}{9}$	0.466	0.311	-	0.461	0.545	

Feb. 2012 (2012-01)	P4	Surface (1-38 m)	22.684	3.765	-	4.592	1.434	0.917	3.781	0.280
		Flux at 50 m	3.283	1.863		0.811	0.122			
		% Flux	14.471	49.468	-	17.668	8.537	-	-	-
	P12	Surface (1-38 m)	11.003	1.425	0.116	5.606	1.894	0.017	1.915	0.500
		Flux at 100 m	0.046	0.020	0.000	0.014	0.005	0.000	0.000	0.000
		% Flux	0.415	1.381	0.000	0.254	0.249	0.000	0.000	0.000
	P26	Surface (1-38 m)	12.161	2.092	1.218	2.923	1.615	0.137	0.902	0.228
		Flux at 100 m	0.380	0.251	0.035	0.046	0.038	0.000	0.014	0.045
		% Flux	3.126	11.999	2.898	1.581	2.373	0.000	1.524	19.919
June 2012 (2012-12)	P4	Surface (1-103 m)	21.313	31.420	-	5.192	-	-	-	-
		Flux at 200 m	1.076	0.919	0.047	0.126	-	-	-	0.036
		% Flux	5.047	2.926	-	2.435	-	-	-	-
	P12	Surface (1-164 m)	27.677	5.967	-	22.445	6.552	-	-	-
		Flux at 200 m	0.051	0.047	-	0.075	0.010	-	0.025	-
		% Flux	0.185	0.787	-	0.335	0.156	-	-	-
	P16	Surface (1-66 m)	12.830	8.722	-	17.321	4.238	-	0.942	0.777
		Flux at 100 m	0.312	0.319	0.045	0.044	0.007	-	-	-
		% Flux	2.431	3.662	-	0.252	0.174	-	-	-
P20	Surface (1-115 m)	18.344	33.038	-	13.892	-	-	13.090	3.538	
	Flux at 100 m	0.016	0.016	0.004	-	0.002	-	0.005	0.001	
	% Flux	0.088	0.049	-	-	-	-	0.036	0.033	
P26	Surface (1-60 m)	14.024	1.977	-	13.572	2.018	-	4.969	2.768	
	Flux at 100 m	0.255	0.304	-	-	0.029	-	0.025	-	
	% Flux	1.821	15.359	-	-	1.437	-	0.507	-	
	Trap (100 m)		0.055	0.025	0.006	0.041	0.004	-	0.009	0.008
		% Flux	0.393	1.243	-	0.304	0.190	-	0.179	0.288

725

726

727

728

Table 4:  $^{234}\text{Th}$  and POC fluxes and POC/ $^{234}\text{Th}$  ratios measured by the PITS traps.

Depth (m)	Days In-situ	$^{234}\text{Th}$ flux (dpm m <sup>-2</sup> d <sup>-1</sup> )	POC flux (mmol m <sup>-2</sup> d <sup>-1</sup> )	POC/ $^{234}\text{Th}$ ratio (μmol dpm <sup>-1</sup> )
June 2011 P26				
30	3.32	3192 ± 117	15.3 ± 0.4	4.8 ± 0.2
50	3.32	2909 ± 92	10.1 ± 0.3	3.5 ± 0.1
100	3.32	2256 ± 94	5.9 ± 0.2	2.6 ± 0.1
150	3.32	1928 ± 79	5.0 ± 0.2	2.6 ± 0.1
200	3.32	2281 ± 97	8.5 ± 0.3	3.7 ± 0.2
June 2012 P26				
30	2.82	3999 ± 206	14.7 ± 0.4	3.7 ± 0.2
50	2.82	5485 ± 290	13.5 ± 0.5	2.5 ± 0.2
100	2.82	3154 ± 192	6.5 ± 0.2	2.1 ± 0.1
150	2.82	2151 ± 135	5.5 ± 0.2	2.5 ± 0.2
200	2.82	3959 ± 129	5.0 ± 0.2	1.3 ± 0.1

729

730

731

732

733

734

735

736

737

738

739

740

741

742

743

744

745

746

747

748 Figure 1. Map showing the Line P stations sampled in this study.  
749

750 Figure 2. Temperature ( $^{\circ}\text{C}$ ), Sigma-t ( $\text{kg m}^{-3}$ ), and  $^{234}\text{Th}/^{238}\text{U}$  activity ratio distributions along  
751 Line P cruises in August 2010, February 2011, June 2011, February 2012, and June 2012.  
752

753 Figure 3. Comparison of small-volume Niskin bottle and large-volume in situ pump  
754 measurements of a) POC, b) picoplankton indicator pigments, c) nanoplankton indicator  
755 pigments, d) microplankton pigments. Niskin bottle measurements are lower than pump  
756 measurements for microplankton pigments, and higher for nanoplankton pigments and POC.  
757

758 Figure 4. a)  $\text{POC}/^{234}\text{Th}$  ratios on 1 – 10- $\mu\text{m}$  particles and on 10 – 53- $\mu\text{m}$  particles plotted against  
759 the  $\text{POC}/^{234}\text{Th}$  ratio on >53- $\mu\text{m}$  particles. Fractional distributions of POC and particulate  $^{234}\text{Th}$   
760 are plotted for three size-classes of particles. The percentage of total POC associated with each  
761 particle size-class is plotted against the percentage of total particulate  $^{234}\text{Th}$  for samples collected  
762 at stations on Line P during b) June 2011, c) February 2012, and d) June 2012. The correlation  
763 coefficient ( $r^2$ ) and the slope of the linear regression ( $m$ ) are shown for each cruise.  
764

765 Figure 5. Pigment Proportion Factors (PF) for each phytoplankton size-class plotted as a  
766 function of sample depth at stations sampled on Line P during the five cruises in the study. All  
767 data were collected from Niskin bottles.  
768

769 Figure 6. Pigment PF for each phytoplankton size group plotted as a function of sample depth  
770 and particle size-class at stations sampled on Line P in June 2011. Size-fractionated data are pump  
771 data. Sediment trap PF's are also included.  
772

773 Figure 7. Pigment PF for each phytoplankton size group plotted as a function of sample depth  
774 and particle size-class at stations sampled on Line P in February 2012. Size-fractionated data are  
775 pump data.  
776

777 Figure 8. Pigment PF for each phytoplankton size group plotted as a function of sample depth  
778 and particle size-class at stations sampled on Line P in June 2012. Size-fractionated data are pump  
779 data. Sediment trap PF's are also included where available.

780

781 Figure 9. Depth profiles of a)  $^{234}\text{Th}$  fluxes ( $P_{Th}$ ) determined using the 2-D model, b)  $\text{POC}/^{234}\text{Th}$   
782 ratios on  $>53\ \mu\text{m}$  particles, and c)  $^{234}\text{Th}$ -derived POC fluxes ( $P_{POC}$ ) at stations on Line P during  
783 the five cruises in this study.

784

785 Figure 10. Net primary production (NPP) plotted against  $^{234}\text{Th}$ -derived POC fluxes ( $P_{POC}$ ) for  
786 stations along Line P in this study. The slopes of the dashed lines represent  $ThE$ -ratios. For  
787 reference NPP and  $P_{POC}$  values determined by Charette et al. (1999) for winter, spring and  
788 summer are included, along with annual average NPP and sediment trap POC fluxes (at 200 m)  
789 reported in Harrison (2002) and Wong et al. (1999) respectively.

790

791 Figure 11. a) Comparison of sediment trap POC fluxes and  $^{234}\text{Th}$ -derived POC fluxes, and b) a  
792 comparison of sediment trap Chl *a* and total indicator pigment fluxes and  $^{234}\text{Th}$ -derived pigments  
793 fluxes at OSP during June 2011 and June 2012.

794

795 Figure 12. a-c)  $^{234}\text{Th}$ -derived indicator pigment fluxes determined using the  $\text{Pigment}/^{234}\text{Th}$  ratio  
796 on  $>53\text{-}\mu\text{m}$  particles plotted for micro-, nano-, and picoplankton pigments. d-f) Indicator  
797 pigment standing stocks plotted against indicator pigment fluxes for micro-, nano-, and  
798 picoplankton pigments. The slopes of the dashed lines indicate pigment loss rates. g-i) The  
799 contribution to total pigment standing stock plotted against the contribution to total pigment flux  
800 for micro-, nano-, and picoplankton pigments. Data points above the 1:1 line indicate  
801 preferential export by direct sinking and points below the 1:1 line indicate disproportionately low  
802 export by direct sinking relative to biomass contributions.

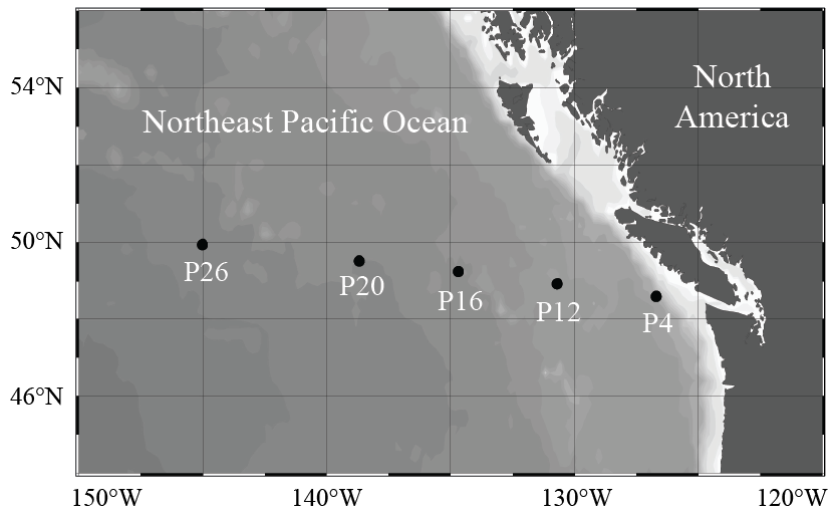
803

804

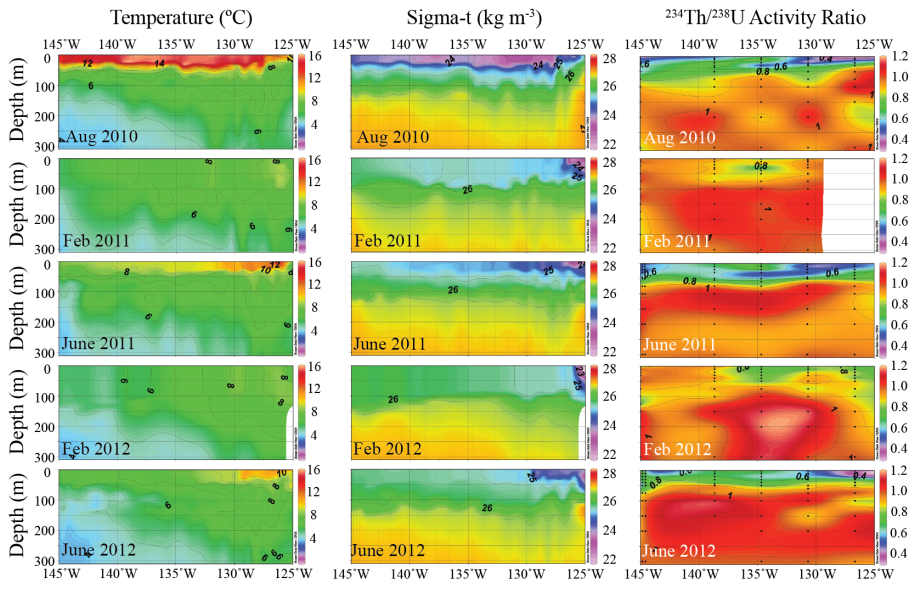
805

806

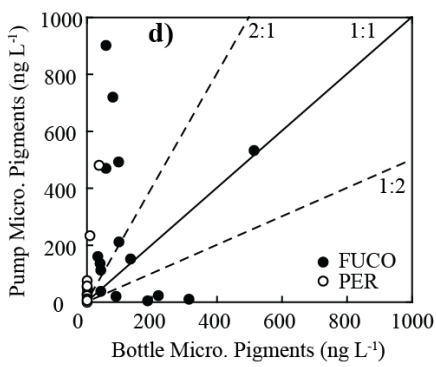
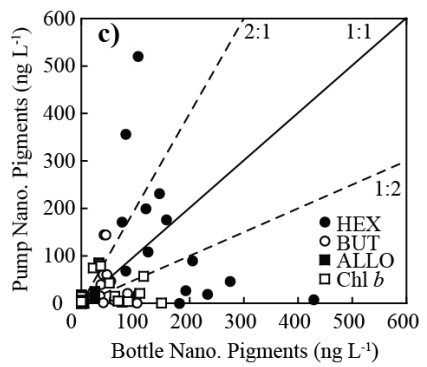
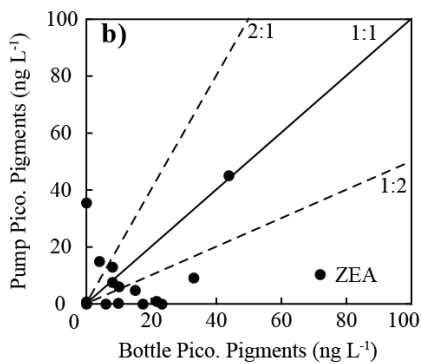
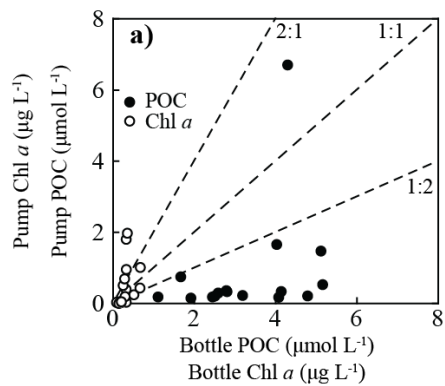
807



808  
809  
810 Fig. 1.  
811  
812  
813  
814  
815  
816  
817  
818  
819  
820  
821  
822  
823  
824  
825

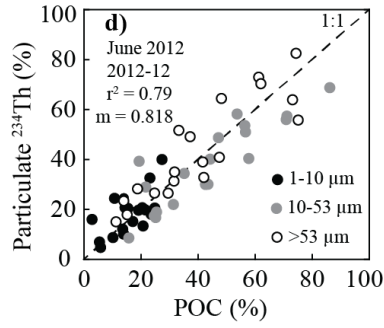
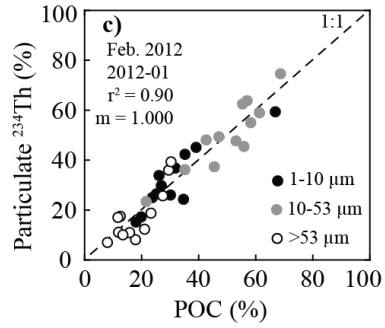
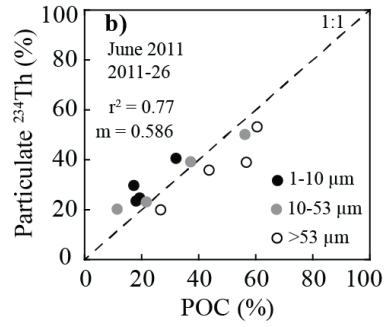
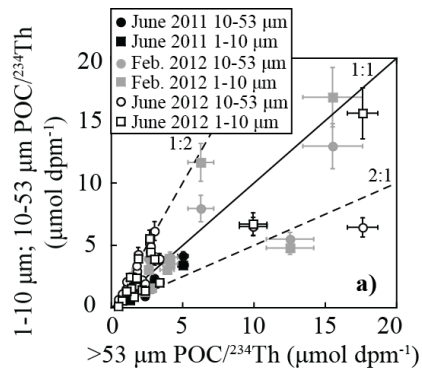


826  
827  
828 Fig. 2.  
829



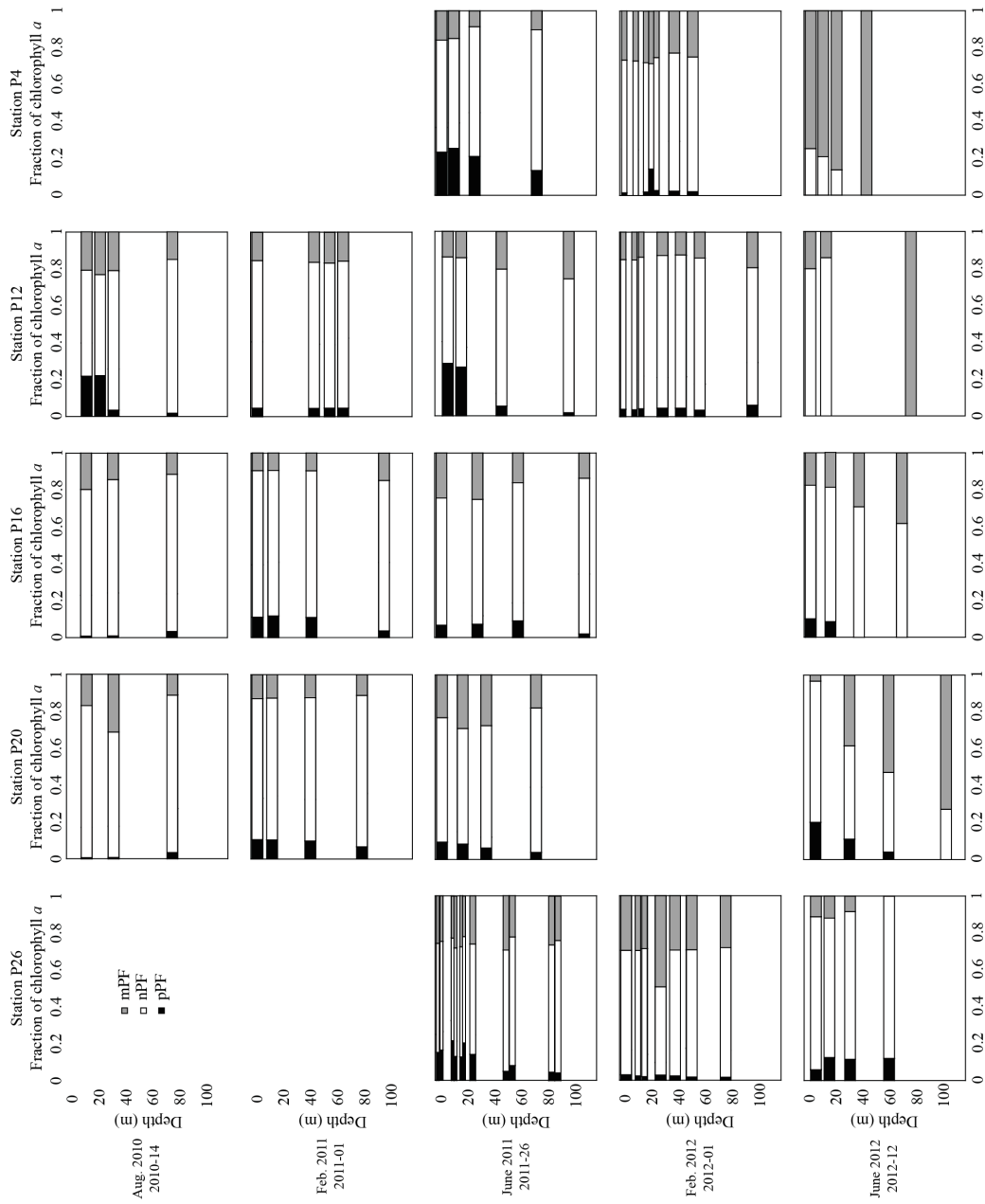
830  
831  
832  
833  
834

Fig. 3.

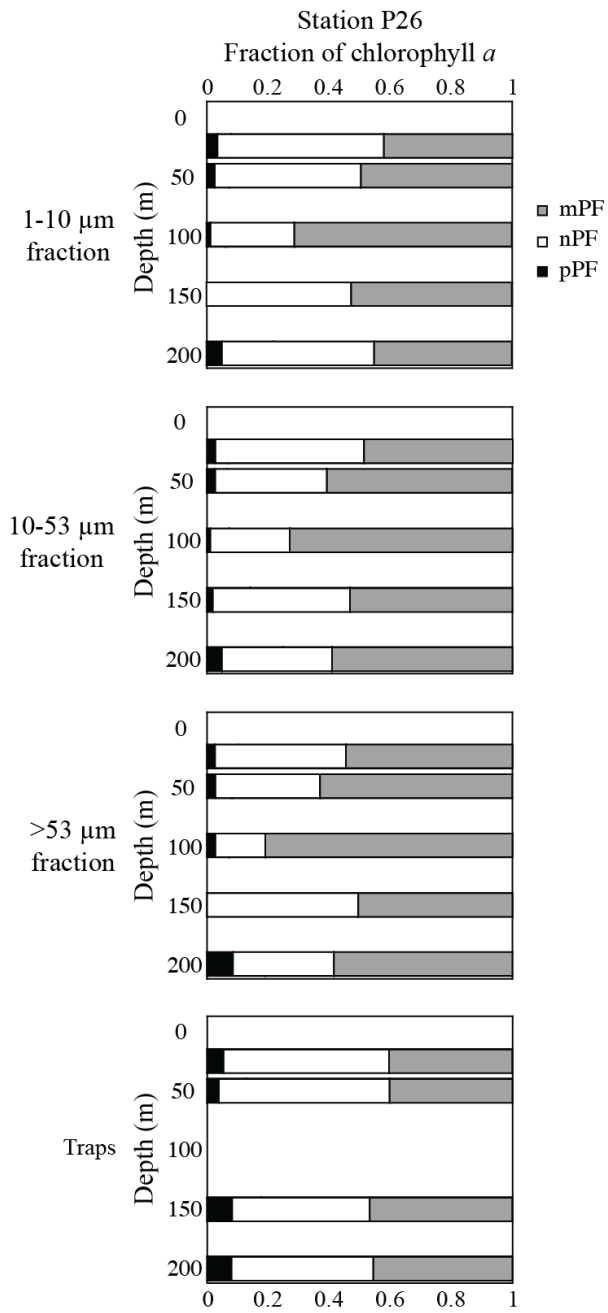


835  
836  
837  
838  
839  
840  
841  
842  
843  
844  
845  
846  
847  
848  
849  
850  
851  
852  
853  
854  
855  
856  
857

Fig. 4.



858  
 859  
 860 Fig. 5.



861  
862 Fig. 6.

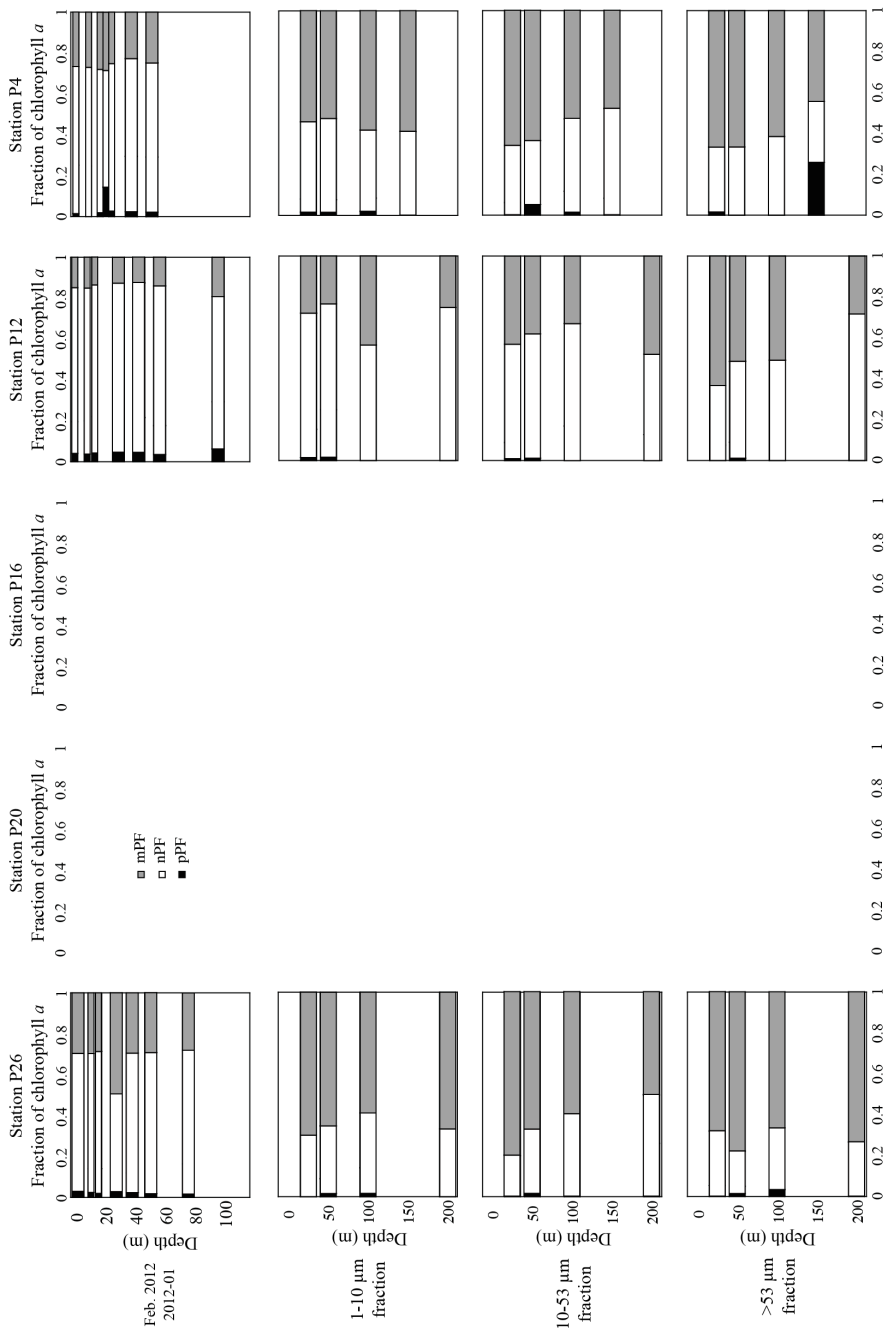


Fig. 7.

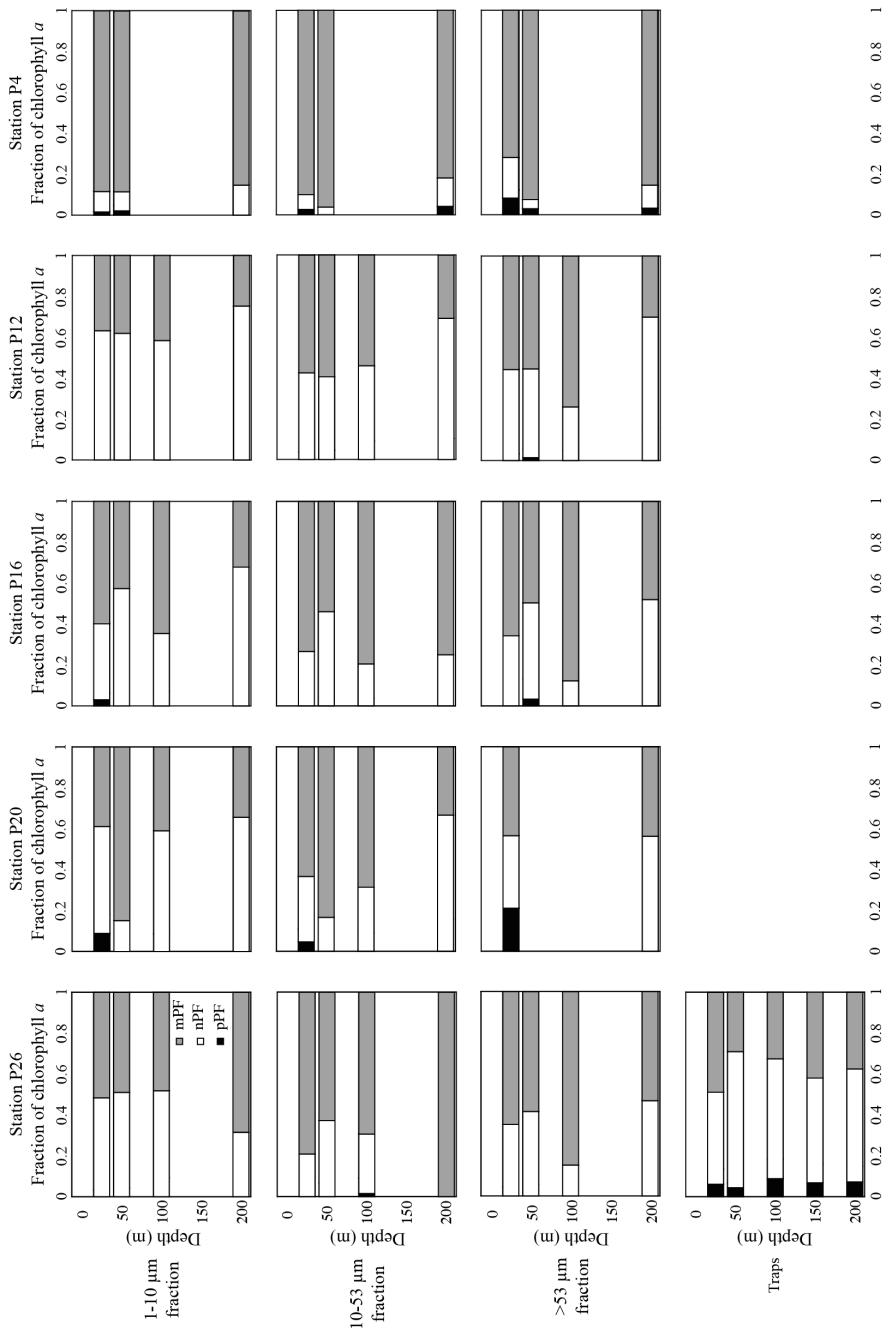
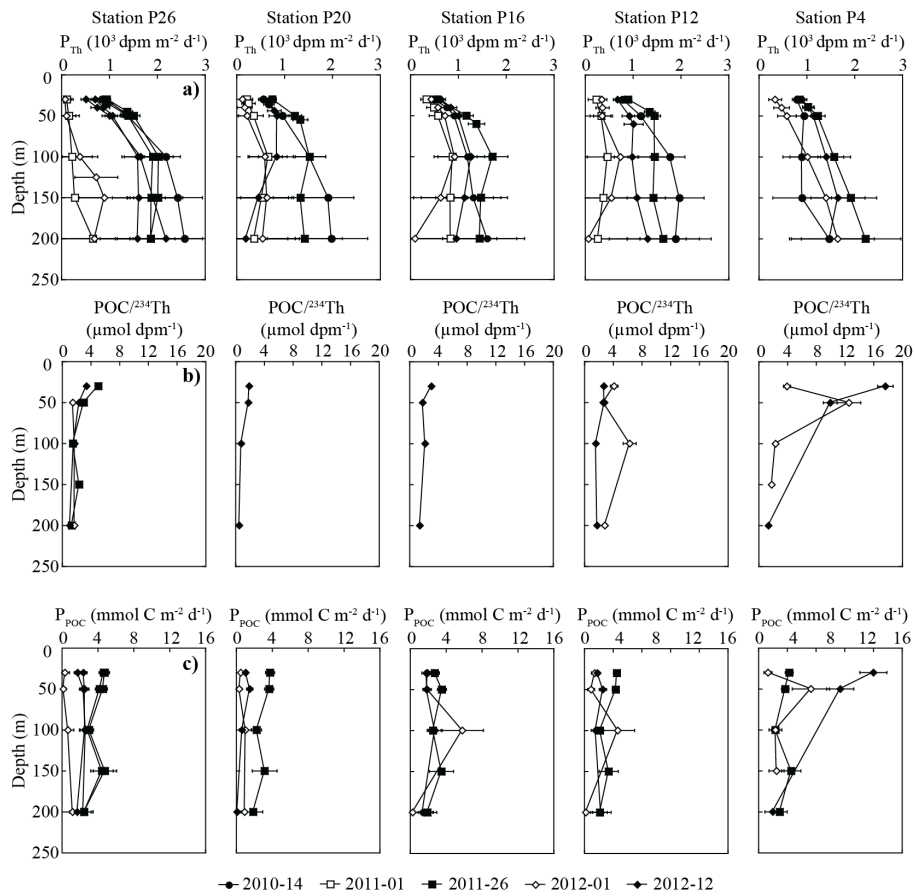


Fig. 8.



865  
 866  
 867  
 868  
 869  
 870  
 871  
 872  
 873  
 874  
 875  
 876  
 877  
 878  
 879  
 880  
 881

Fig. 9.

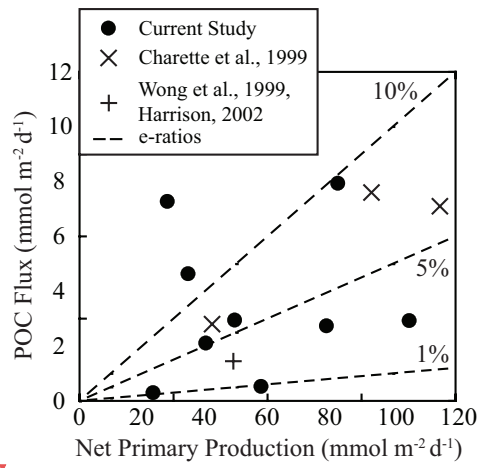
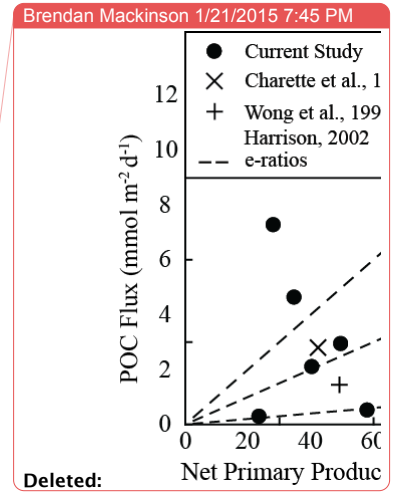
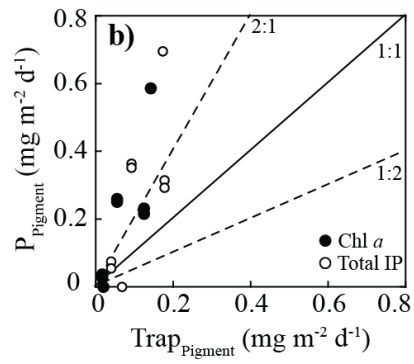
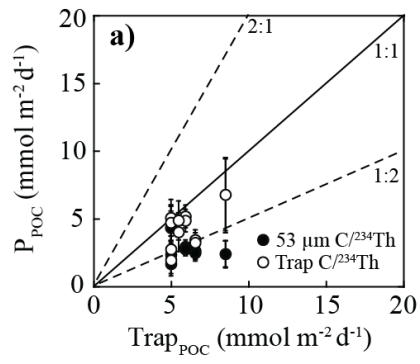


Fig. 10.

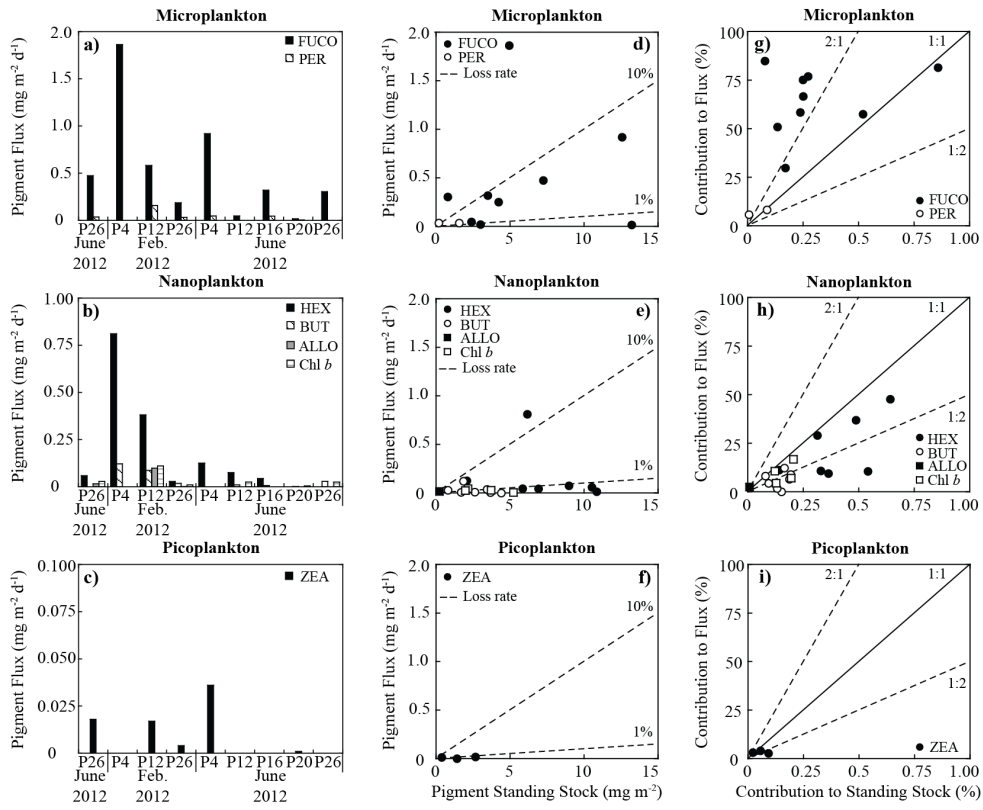


Deleted:

882  
883  
884  
885  
886  
887  
888  
889  
890  
891  
892  
893  
894  
895  
896  
897  
898  
899  
900  
901  
902  
903



905  
 906  
 907 Fig. 11.  
 908  
 909  
 910  
 911  
 912



913  
914  
915 Fig. 12.